Received: 22 August 2023 | Revised: 31 March 2024 | Accepted: 4 April 2024

DOI: 10.1002/joc.8462

RESEARCH ARTICLE

International Journal of Climatology RMetS

Orographic effects on droughts in a monsoon climate with the world's highest rainfall

Paweł Prokop[1] | **Adam Walanus**[2]

[1]Department of Geoenvironmental Research, Institute of Geography and Spatial Organization, Polish Academy of Sciences, Kraków, Poland

[2]Faculty of Geology, Geophysics and Environmental Protection, AGH University of Science and Technology, Kraków, Poland

Correspondence
Paweł Prokop, Department of Geoenvironmental Research, Institute of Geography and Spatial Organization, Polish Academy of Sciences, Jana 22, 31-018 Kraków, Poland.
Email: pawel@zg.pan.krakow.pl

Abstract

Drought, a recurring natural phenomenon in South Asia's monsoon climate, presents challenges in delineating its spatiotemporal patterns within complex topographies. This study investigated the impact of the orographic barrier in the rice-dominated agricultural region of northeastern India and Bangladesh on drought characteristics during 1951–2020, employing the relative Standardized Precipitation Index (rSPI) and relative Standardized Precipitation-Evapotranspiration Index (rSPEI) across 3-, 6- and 12-month scales. The results indicate that even in the rainiest region of the world, droughts extend beyond the limits of the dry season inherent in the monsoon regime. These mostly regional droughts exhibit weak correlations with the core of the Indian subcontinent and other parts of Bangladesh. The region's orographic barrier has a greater influence on drought intensity than on frequency. The rSPI index, which depends solely on rainfall, may overestimate drought intensity and frequency in regions with high seasonal/annual rainfall and substantial intermonthly variability. In contrast, the rSPEI index, which depends on both rainfall and potential evapotranspiration (PET), better reflects the spatial variation of drought in complex terrain, identifying the leeward hinterland of the orographic barrier as the most drought-prone area. The two indices give similar results for drought characteristics away from the barrier. Furthermore, the orographic barrier exerts a negligible influence on the trends in rSPI and rSPEI. Principal component analysis (PCA) highlights the influences of the rainfall coefficient of variation and elevation on rSPI, while the PET coefficient of variation strongly influences rSPEI. Strategies to minimize the adverse effects of drought in complex topography and year-round cropping should be local and season-specific. These include using shorter-growing, drought-resistant rice varieties and adjusting planting schedules in rain shadow areas during the summer monsoon. These efforts should be complemented by integrating indigenous irrigation methods with modern practices such as roof water harvesting and tube wells in winter.

KEYWORDS

drought, orographic rainfall, relative drought index, spatiotemporal variation, topography

1 | INTRODUCTION

The Asian monsoon climate is characterized by distinctly wet summers and dry winters, driven by the migration of the Intertropical Convergence Zone (ITCZ) and the annual reversal of wind patterns (Gadgil, 2003; Hari et al., 2020). Variability in the position of the ITCZ can lead to temporal rainfall deficits and drought through the delay, early withdrawal, or reduction of summer monsoon rainfall (Mahto & Mishra, 2020; Misra et al., 2018). Apart from the annual variability, the ITCZ also experiences intraseasonal variability in its position and intensity (Samuel et al., 2023). Coupled with such intraseasonal variability, active (wet) and break (dry) phases of monsoon rainfall can influence the occurrence of drought (Roman-Stork et al., 2020). Active and break phases are largely controlled by the most prominent quasi-bi-weekly oscillation with a period of 7–25 days and a Madden–Julian oscillation with a period of 30–60 days (Dey et al., 2022; Goswami & Mohan, 2001). In particular, the submonthly oscillation associated with the north–south movement of the monsoon trough is significantly more robust than the Madden–Julian oscillation associated with the northward propagation of convection from the equatorial Indian Ocean (Fujinami et al., 2011). The consequences of droughts can be more disastrous when they coincide with heat extremes, leading to soil moisture depletion (Mishra, 2020b). Dry soils increase the likelihood of simultaneous hot and dry extremes by reducing evaporation and increasing atmospheric heating. In effect, the combination of enhanced land–atmosphere feedback and intraseasonal variability in summer monsoon rainfall may increase the risk of droughts (Mahto & Mishra, 2023; Mukherjee & Mishra, 2021).

South Asia, within the range of the monsoonal circulation, has a diverse climate because of its vast size and varied topography; therefore, different climate types contribute in different ways to the occurrence and intensity of drought (Krishnan et al., 2020; Raju et al., 2013). Northwestern India, with tropical arid (Köppen classification BW) and semi-arid (BS/BSh) climates, experiences inherently high temperatures and limited rainfall. In contrast, most of India and Bangladesh, with tropical monsoon (Am) climates, suffer from uneven distribution and variability of rainfall. Subtropical (Cwa) highlands are often affected by orographic effects that can either exacerbate or alleviate drought. In particular, orographic barriers oriented perpendicular to the prevailing direction of air masses disrupt atmospheric stratification and enhance the spatial distribution of precipitation (Roe, 2005). While there is some overlap in the physical principles of orographic lift and rain shadow effects in all climate zones (Chao, 2012; Rotunno & Houze, 2007), the specific behaviour and effects of orography in monsoonal climates differ because of the unique seasonal and regional characteristics of monsoon (Anders et al., 2006; Bookhagen & Burbank, 2006; Kad & Ha, 2023; Kumari et al., 2017; Tawde & Singh, 2015; Xie et al., 2006). Orographic effects in monsoonal regions are closely linked to the reversal of prevailing wind patterns. During the rainy season, moist air rises over the mountains, resulting in increased rainfall on the windward side and rain shadows on the leeward side. Conversely, in the dry season, when the wind direction changes, the rain shadow effect can occur on the side that received more rainfall in the previous season. Orographic barriers amplify differences in rainfall variability as well as evapotranspiration rates influenced by seasonal and altitudinal temperature changes (Stevens, 2005), resulting in adjacent areas experiencing both water surpluses and shortages (Houze Jr., 2012). Therefore, orographic influences on drought in monsoonal climates are highly localized in space and time, and the magnitudes of the influences depend on the topography of the region (Fahad et al., 2022).

The increased spatial and temporal variability of rainfall and temperature, driven by topographic features, facilitates the emergence of meteorological drought, which serves as the first indication of a temporary deficit of rainfall (Haile et al., 2020; Wilhite & Glantz, 1985). Prolonged meteorological droughts can escalate into agricultural, hydrological and socioeconomic droughts, affecting water-related activities. Given the complex nature of climate-related hazards, numerous indices have been proposed to characterize drought conditions quantitatively (Mishra & Singh, 2010; Svoboda & Fuchs, 2016). The Palmer Drought Severity Index (PDSI; Palmer, 1965) and the Deciles (Gibbs & Maher, 1967) were among the earliest drought indices developed and used for drought monitoring. However, it was not until the development of the Standardized Precipitation Index (SPI; McKee et al., 1993) that the relationship between drought and its frequency and duration at different time scales could be established (Guttman, 1998). The methodological concept of the SPI calculation inspired the development of the analogous Standardized Precipitation-Evapotranspiration Index (SPEI; Vicente-Serrano et al., 2010), which is based on both precipitation and potential evapotranspiration (P-PET). In recent decades, the SPI and SPEI have become among the most widely used indices in various climatic zones, including monsoonal climates (Chandrasekara et al., 2021; Uddin et al., 2020). The SPI is a suitable tool for assessing drought in monsoonal climates with distinct wet and dry seasons because it takes into account the seasonality of precipitation by assessing how current precipitation compares to the historical record for the same time

of year, offers flexibility in time scales that can be adapted to both the different lengths of seasons and the different response times of different drought types, and provides standardized values for ease of interpretation (Hayes et al., 1999). The SPEI, in addition to having advantages similar to those of the SPI, is suitable for monsoon regions with complex topography that often experience high temperatures and intense solar radiation, as well as changes in temperature with elevation, leading to significant variations in evapotranspiration patterns (Wable et al., 2019).

While such index-based approaches are effective in assessing drought, the SPI and SPEI define meteorological droughts based on standardized precipitation deficits relative to historical local conditions over a specified time period (Hayes et al., 1999; Vicente-Serrano & Beguería-Portugués, 2003). Consequently, the frequency of droughts remains largely uniform across stations, regardless of climate and rainfall. Recognizing these limitations, Dubrovsky et al. (2009) introduced the relative SPI (rSPI) drought index, calibrated using reference station data or averaged precipitation from multiple stations (Trnka et al., 2009). A similar approach was adopted for the relative SPEI (rSPEI; Marcos-Garcia et al., 2017; Feng et al., 2019), which facilitates absolute drought comparisons between stations and nuanced distinctions between them.

The border region of northeastern India and Bangladesh is a striking example of complex and extensive spatiotemporal rainfall variability on a global scale (Goswami et al., 2010). Because of the forced ascent of moisture-laden air masses, the southern escarpment of the Meghalaya Plateau receives 12,000 mm of rainfall annually, creating a distinct boundary between the humid Bengal Plain and the comparatively arid northern slope of the plateau along the Brahmaputra Valley (Ahmed et al., 2022; Kuttippurath et al., 2021). Consequently, different topographies within this region, each characterized by unique climatic conditions, may have different vulnerabilities to drought events. Previous climate studies in northeastern India and Bangladesh have predominantly focused on extreme rainfall, its variability associated with intraseasonal oscillations, and its role in triggering widespread flooding across the Bengal Plain (e.g., Fujinami et al., 2014; Hofer & Messerli, 2006; Mahanta et al., 2013; Murata et al., 2017; Varikoden & Revadekar, 2020). In northeastern India, drought research has focused on the spatiotemporal variability of SPI and SPEI, often in the context of national policy for India as a whole (Kumar et al., 2012, 2013), meteorological subdivisions (Acharya et al., 2013; Shahfahad Talukdar et al., 2023) and homogeneous rainfall regions (Das et al., 2016). These studies used gridded rainfall and temperature datasets for the summer monsoon with spatial resolutions of $1 \times 1^\circ$ or $0.5 \times 0.5^\circ$ or station-based rainfall data. District-level drought assessments have also been conducted using averaged rainfall data from stations at the smallest administrative unit level and the SPI (Guhathakurta et al., 2017; Pai et al., 2011). In addition, several studies have addressed drought assessment in Bangladesh using the same drought indices derived from interpolated data from multiple stations across the country (e.g., Alamgir et al., 2019; Kamruzzaman et al., 2022; Miah et al., 2017; Mondol et al., 2017; Rahman et al., 2021).

A review of the literature highlights the predominant focus of drought analyses on the summer monsoon season, overlooking the wettest districts and the region's exposure to sporadic tropical cyclones and local convection accompanied by intense thunderstorms during the rest of the year (Alam et al., 2003; Mahanta et al., 2013; Singh et al., 2011). The use of relatively coarse gridded data or averaged data from multiple stations at the smallest administrative unit level may not capture the nuances of spatial rainfall variation, especially in hilly areas. Furthermore, the traditional SPI and SPEI indices may not be sufficiently sensitive to detect relatively small areas of extreme wet and dry conditions because of their uniform frequency among locations over long periods of time.

Our study addresses these gaps in the literature, focusing on the less explored understanding of orographic effects on drought frequency and intensity in a monsoon climate with the highest rainfall in the world. Emphasizing the importance of considering both climate seasonality and topographic complexity in drought assessments, we highlight the differential vulnerability to drought events across an orographic barrier. Recognizing the limitations of traditional drought indices, our research adopts the relative rSPI and rSPEI as innovative tools tailored to assessing drought in regions with complex topography. This novel approach, calibrated using averaged rainfall from multiple stations, allows for a more nuanced and site-specific assessment of drought conditions and allows for absolute comparisons between stations. Addressing the aforementioned shortcomings is critical as agricultural losses due to drought exceed those due to floods in the region with the world's highest rainfall (Vishnu et al., 2022; World Bank Bangladesh, 1998).

The aim of this study was to assess the orographic barrier effect on the spatial and temporal characteristics of droughts in the world's highest-rainfall region—northeastern India and Bangladesh—over the period 1951–2020. Specifically, the objectives were: (i) to use rSPI and rSPEI as relative indicators of drought to examine their effectiveness in delineating drought characteristics between stations located along the orographic barrier, and (ii) to identify the primary drivers of drought occurrence.

2 | MATERIALS AND METHODS

2.1 | Study area

2.1.1 | Mechanism of orographic rainfall and the role of elevation in rainfall distribution

The study area is located in the border region between northeastern India and Bangladesh (Figure 1), which is renowned for having the highest rainfall recorded in the world. The southwest monsoon in this area exhibits weak correlations or phase differences compared to the rest of India (Choudhury et al., 2021; Rajesh et al., 2021). This distinctive behaviour is accompanied by pronounced spatiotemporal variability in rainfall, a result of complex interactions between the monsoon circulation and the local topography. Observations of the 925-hPa circulation indicate that moisture is transported from the northern Bay of Bengal towards India and Bangladesh by the enhanced low-level jet (Fujinami et al., 2022; Sato, 2013). This strengthening of the winds is attributed to monsoonal differential heating, which creates a stronger land–sea thermal contrast and drives moisture circulation towards the north. Convective cells associated with the Bay of Bengal depression evolve into mesoscale convective systems near the Meghalaya Plateau, which rises approximately 2 km above the surrounding lowlands. The plateau acts as an east–west orographic barrier and plays a crucial role in forcing moisture to precipitate by convergence.

The elevation of the Meghalaya Plateau has a significant influence on the distribution, intensity and variability of rainfall. On the steep southern slope of the plateau, annual rainfall increases by an average of approximately 500 mm per 100 m of elevation, reaching a maximum at Cherrapunji (Murata et al., 2017) (Table 1). The surface of the plateau is characterized by relatively flat terrain with scattered hills. In this area, rainfall decreases rapidly with distance from the southern edge, and there is no discernible relationship between elevation and rainfall. In contrast, the northern slope of the plateau has a more gentle profile, with a recorded decrease in annual rainfall of approximately 26 mm per 100 m of elevation between Shillong and Gauhati. The impact of elevation on annual rainfall variability across the orographic barrier is also evident, with higher elevation stations, particularly Cherrapunji, showing the highest coefficients of variation (Figure 2). Over the course of the year, the lowest coefficients of variation for rainfall are recorded during the summer monsoon months, while the peak is observed during the latter stages of the post-monsoon season and the winter. In contrast, annual potential evapotranspiration (PET) shows minimal variability compared to rainfall, with month-to-month variations at specific stations rarely exceeding 5%.

2.1.2 | Climatic, topographic and agricultural conditions across the orographic barrier

The drought analysis was conducted using data from four climatological stations located along the dominant south–north (S–N) trajectory of the monsoonal circulation across the Meghalaya Plateau (Figure 1 and Table 1). These stations represent different topographic and climatic conditions, covering the Bengal Plain (Sylhet), the hilly terrain of the Meghalaya Plateau (Cherrapunji and Shillong) and the flat Brahmaputra Valley (Gauhati). Sylhet and Cherrapunji, located on the foreland and southern crest of the plateau, respectively, typify the windward side of the orographic barrier. In contrast, Shillong and Gauhati, located on the northern slope of the plateau and in the lowlands, respectively, exemplify the leeward side (rain shadow) during the southwest monsoon.

The study area has a subtropical monsoon climate, classified as Cwa for the lowlands and Cwb for the plateau. In general, the mean annual air temperature decreases with increasing altitude. An exception is Cherrapunji, which receives less sunshine during the summer monsoon, resulting in a comparatively lower mean annual temperature than Shillong at higher elevations. Typically, the onset of the summer monsoon enveloping the region occurs in early June, while the withdrawal of monsoonal influence occurs around mid-October (Pai et al., 2020). It is noteworthy that, on average, a substantial proportion—approximately 68%—of the annual rainfall occurs during the June–September southwest monsoon season. The winter months (January and February) are relatively dry and cool.

Administratively, the study area covers two Indian states, Meghalaya (Cherrapunji, Shillong) and Assam (Gauhati), and the Sylhet Division of Bangladesh. The region is characterized by subsistence farming and the dominance of rainfed agriculture (Vaid, 2020). Rice is the main crop, while tea, jute, potato, ginger and oilseeds are the major cash crops. Rain-fed crops are sown in summer (June–July) and harvested in autumn (September–October), while irrigated crops are sown in winter (October–December) and harvested in spring

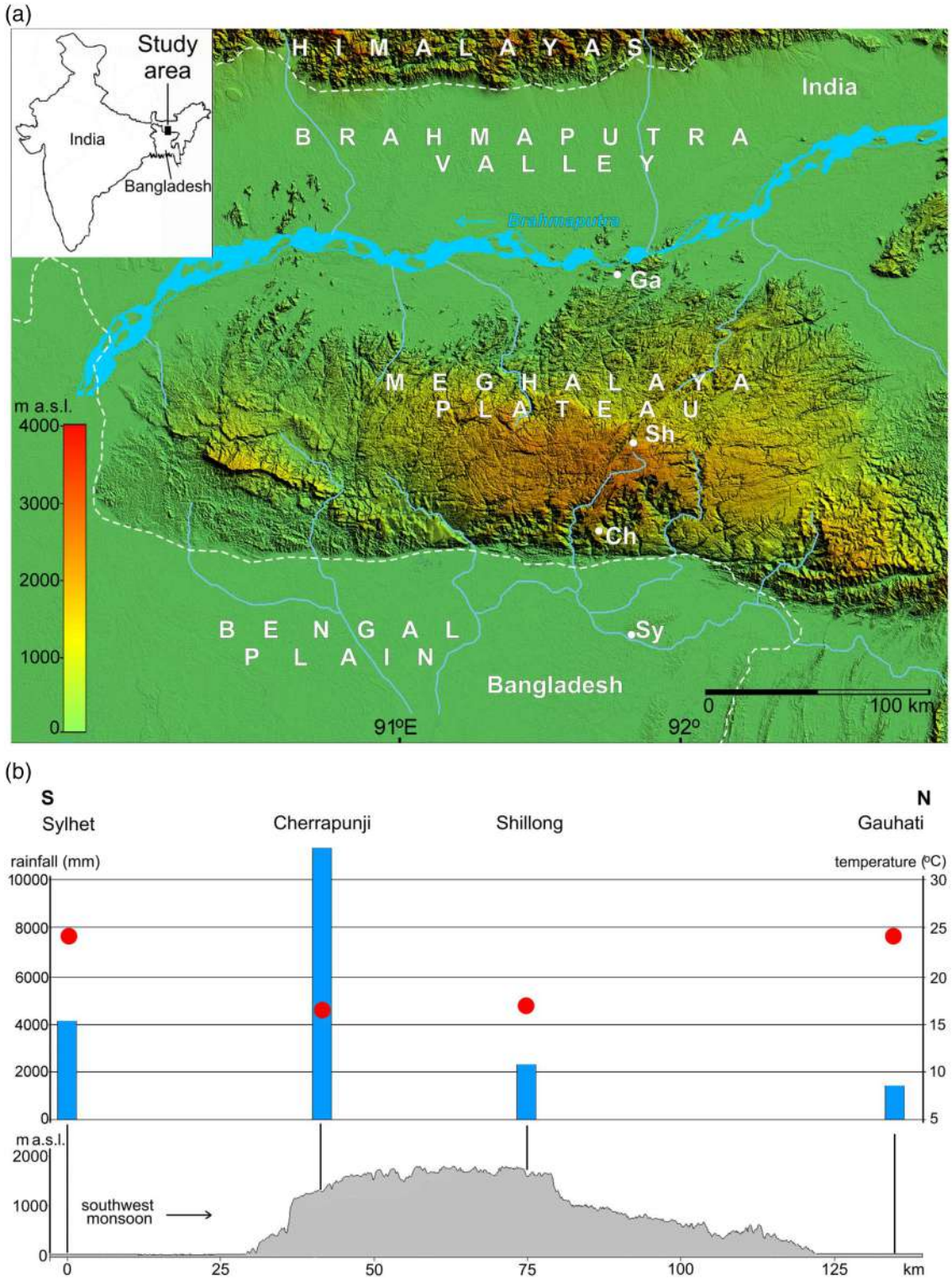

FIGURE 1 Study area (a) locations of the Sylhet (Sy), Cherrapunji (Ch), Shillong (Sh) and Gauhati (Ga) stations and (b) spatial distribution of mean annual temperature (red dots) and mean annual rainfall (blue bars) along the S–N trajectory across the orographic barrier in northeastern India and Bangladesh during 1951–2020. [Colour figure can be viewed at wileyonlinelibrary.com]

(March–April) (Alamgir et al., 2015; Prokop et al., 2018). Agricultural land in the region is irrigated by surface water in parts of India and by groundwater in parts of Bangladesh.

2.2 | Data collection

The analysis of droughts in this study is based on a comprehensive dataset spanning 70 years (1951–2020) of

TABLE 1 Meteorological stations in the study area.

Station	Lat. (°)	Lon. (°)	Elevation (m a.s.l.)	Mean annual temperature (°C)	Mean annual rainfall (mm)	Rainfall coef. of variation (%)	PET (mm)	PET coef. of variation (%)	PET contribution to annual rainfall (%)	Koppen climate type
Sylhet	24.9	91.9	34	24.6	4078.9	100	1201.0	22	29.4	Cwa
Cherrapunji	25.3	91.7	1313	16.9	11596.1	121	884.8	24	7.6	Cwb
Shillong	25.6	91.9	1598	17.6	2166.3	110	898.4	28	41.5	Cwb
Gauhati	26.1	91.6	54	24.7	1677.7	100	1186.9	26	70.7	Cwa

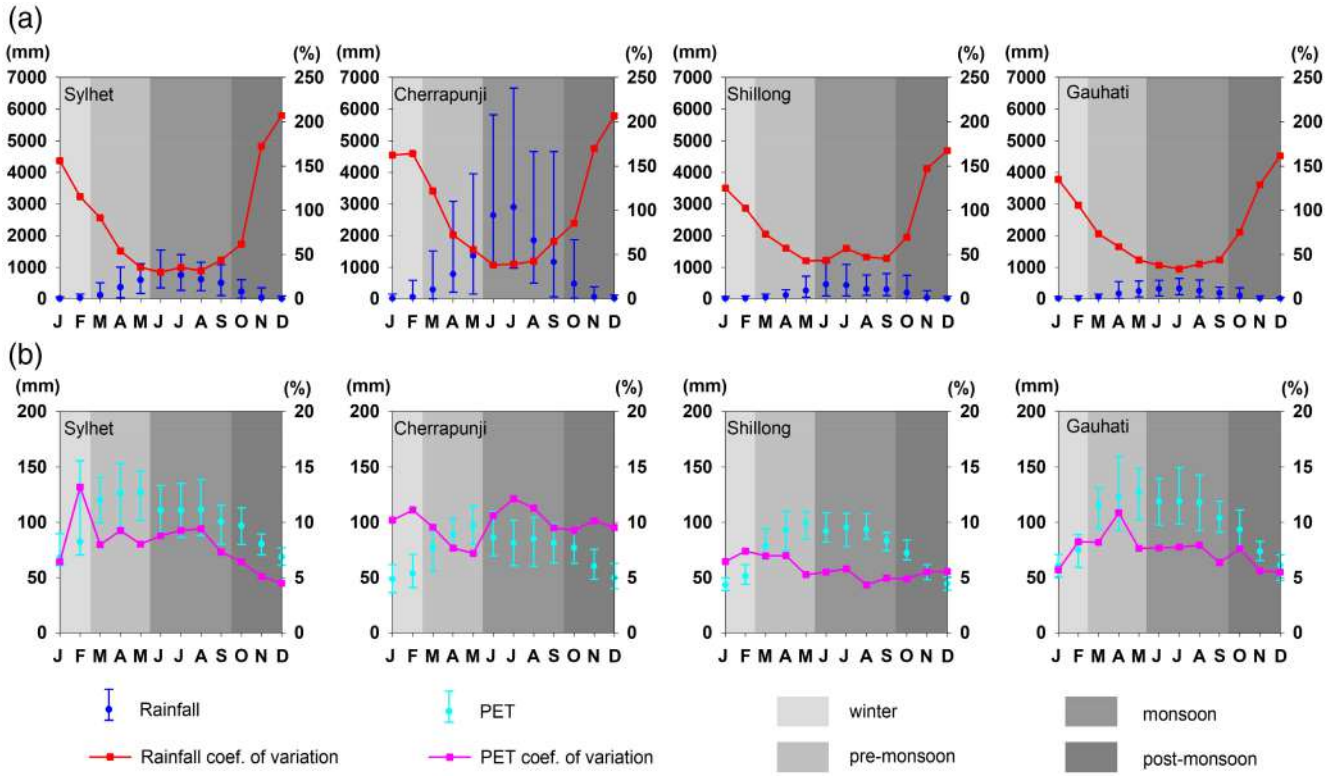

FIGURE 2 Monthly distributions of minimum, mean and maximum (a) rainfall (mm) and its coefficient of variation (%) and (b) PET (mm) and its coefficient of variation (%) across the orographic barrier during 1951–2020 used to calculate rSPI and rSPEI. [Colour figure can be viewed at wileyonlinelibrary.com]

monthly observations from four different stations. Monthly records of rainfall, minimum and maximum temperatures were collected from the National Data Centre of the Indian Meteorological Department, covering Cherrapunji, Shillong and Gauhati. Data for Sylhet were obtained from the Bangladesh Meteorological Department. In addition, some data were collected directly from the stations during extensive fieldwork conducted between 2000 and 2018. Missing values were correlated with data from neighbouring stations to fill gaps in the climatological data. Historical annual archives from the Indian Meteorological Department were also consulted to supplement the data set.

2.3 | Drought analysis

2.3.1 | Calculation of drought indices

The pronounced spatial variability of topographically influenced rainfall over a limited area led us to adopt the relative versions of the standardized indices, namely rSPI and rSPEI (Dubrovsky et al., 2009), instead of the traditional SPI and SPEI for drought assessment. The detailed methods for calculating the traditional SPI and SPEI are comprehensively described by McKee et al. (1993) and Vicente-Serrano et al. (2010), as well as subsequent works

(e.g., Beguería et al., 2014; Guttman, 1999). Consequently, we briefly describe the methods and distinctions between traditional and relative index calculations. To calculate the original SPI and SPEI, the precipitation and P–PET series for an individual site (station) are fitted to a probability distribution. The probabilities are then transformed to a normal distribution to derive SPI and SPEI values. This procedure uses the same precipitation and P–PET series separately for each month and site. In contrast, the calculation of rSPI and rSPEI involves generating reference P and P–PET series, respectively, by averaging monthly precipitation and P–PET totals from the four stations (Dubrovsky et al., 2009; Feng et al., 2019; Marcos-Garcia et al., 2017; Trnka et al., 2009) (Table 2, equations (1)–(12)). A gamma distribution (for rSPI) and a log-logistic distribution (for rSPEI) were fitted over the 1951–2020 baseline to determine the relative standardized indicators. These distributions are widely used in the literature and endorsed by their original developers. The calculation of potential evapotranspiration was performed using the temperature-based Penman–Monteith equation (Allen et al., 1998), derived by the United Nations' Food and Agriculture Organization (FAO) due to the lack of long-term data on solar radiation, humidity and wind speed. Various studies conducted under different climatic conditions (López-Moreno et al., 2009), including the Meghalaya Plateau (e.g., Pandey & Pandey, 2016), have demonstrated the applicability of this method for characterizing drought using SPEI, with limited discrepancies compared to the FAO Penman–Monteith equation.

In this study, we calculated rSPI and rSPEI at 3-, 6- and 12-month time scales, which correspond to different patterns of rainfall deficit (Mishra & Singh, 2010). The 3-month scale relates primarily to meteorological drought, which affects agricultural activities through soil moisture and crop stress. Longer time scales of 6–12 months are more appropriate for assessing hydrological drought, which includes river discharge or groundwater availability, and are better suited to identifying prolonged dry spells. Negative values of rSPI and rSPEI denote rainfall deficiency (below the mean rainfall), whereas positive values signify a surplus of rainfall (above the mean). Drought classification for both rSPI and rSPEI uses a consistent scale that divides conditions into seven distinct rainfall regimes, ranging from extremely wet (≥ 2) to extremely dry (≤ -2), with gradations of very wet (1.5–1.99), moderately wet (1–1.49), normal (−0.99 to 0.99), moderately dry (−1 to −1.49) and severely dry (−1.5 to −1.99) between those two extreme regimes (Hayes et al., 1999).

The application of runs theory was used to describe the intensity, frequency, and duration of droughts (Yevjevich, 1967). In this context, the duration of a drought episode is defined as the period during which the rSPI or rSPEI reaches a value of −1.00 or less and persists until positive values reappear (Liu et al., 2021; Mishra & Singh, 2010). The drought severity is reflected by the cumulative deficit of rSPI or rSPEI values that fall in the range ≤ 1. Drought intensity is derived by dividing the drought severity by the drought duration, while drought frequency is calculated by dividing the number of droughts (n) by the time period (N) (Table 2, equations (13) and (14)).

Bayes' theorem was used to determine the conditional probability of event A, given the occurrence of event B (CP(A|B)). In this study, Cp(rSPEI) refers to the probability of an rSPEI drought episode occurring during an rSPI drought episode (Table 2, equation (15)).

2.3.2 | Trend analysis

The original Mann–Kendall (M–K) trend test is based on a rank correlation analysis of observations and their temporal order (Kendall, 1975; Mann, 1945) (Table 2, equations (16)–(18)). The M–K test is robust because it does not assume a specific probability distribution for the data. This is advantageous when dealing with data sets that deviate from a normal distribution or contain outliers. This test is widely accepted in the field of climatology and is endorsed by the World Meteorological Organisation (Sneyers, 1990).

The presence of positive autocorrelation in the data increases the likelihood of detecting trends where none exist and vice versa. As the rSPI and rSPEI series are autocorrelated, a correction is necessary. In the present study, a modified M–K trend test was used to identify monotonic trends in rSPI and rSPEI at each station over time scales of 3, 6 and 12 months to mitigate problems associated with autocorrelation. This version is based on the adjusted variance of $S(\mathrm{var}^*(S))$, as proposed by Yue and Wang (2004) (Table 2, equations (19) and (20)).

The M–K test determines the direction of the trend. To measure the magnitude of the trend, linear trend analysis was then applied using Sen's slope (Sen, 1968) (Table 2, equation (21)). Sen's slope serves as a nonparametric tool to quantify both the magnitude and direction of trends (Liu et al., 2021).

2.3.3 | Principal component analysis

Principal component analysis (PCA) was performed to reduce the dimensionality of the datasets and identify

TABLE 2 Steps to calculate rSPI, rSPEI and their parameters.

rSPI	rSPEI
(1) Establishment time series *X* for different monthly time scales *k*	
In order to obtain a mean precipitation series that is useful for summing up four series of very different precipitation, it is almost necessary to standardize the series before summing them up, i.e., to carry out a transformation: $y_i = (x_i - av(x))/\mathrm{sd}(x)$.	
$P_{i,m}$, (1)	$D_{i,m} = P_{i,m} - \mathrm{PET}_{i,m}$, (2)
where i is year m is month in year	
	where PET is the potential reference evapotranspiration ($\mathrm{mm \cdot month^{-1}}$; Allen et al., 1998), $\mathrm{PET} = \frac{0.408\Delta(R_n - G) + \gamma\frac{900}{T+273}u_2(e_S - e_a)}{\Delta + \gamma(1 + 0.34u_2)}$, (3) where R_n is the net radiation at the crop surface ($\mathrm{MJ \cdot m^{-2} \cdot month^{-1}}$), G is the soil heat flux ($\mathrm{MJ \cdot m^{-2} \cdot month^{-1}}$), T the mean air temperature at 2 m height (°C), u_2 the wind speed at 2 m height ($\mathrm{m \cdot s^{-1}}$), e_S the saturated vapour pressure (kPa), e_a the actual vapour pressure (kPa), Δ the slope vapour pressure curve ($\mathrm{kPa \cdot {}^\circ C^{-1}}$), γ is the psychometric constant ($\mathrm{kPa \cdot {}^\circ C^{-1}}$). The values of e_S, e_a, R_n, G, Δ, γ, data were estimated from maximum, and minimum temperatures $T_{\max}$ and $T_{\min}$, the altitude of the station and the latitude of the location.
$X_{i,m}^k = \sum_{t=13-k+m}^{12} P_{i-1,t} + \sum_{t=1}^{m} P_{j,t}$, (4)	$X_{i,m}^k = \sum_{t=13-k+m}^{12} D_{i-1,t} + \sum_{t=1}^{m} D_{j,t}$, (5)
where k is the time scale i is the year, m is the month in year, P is precipitation.	
(2) Fitting distribution function for time series *X*	
Fitting of a two-parameter gamma distribution and calculating of its cumulative probability distribution function (Dubrovsky et al., 2009; McKee et al., 1993).	Fitting of a three-parameter log-logistic distribution and calculating of its cumulative probability distribution function (Marcos-Garcia et al., 2017; Vicente-Serrano et al., 2010).
$G(x) = \int_0^x \frac{1}{\Gamma(\alpha)\beta^\alpha} x^{\alpha-1} e^{-x/\beta} dx$, (6)	$F(x) = \left[1 + \left(\frac{\beta}{x-\gamma}\right)^\alpha\right]^{-1}$, (7)
where α is the shape parameter, β is the scale parameter.	where α is the shape parameter, β is the scale parameter and γ is the origin parameter.
(3) Calculation of the gamma cumulative probability of a time series *X* in the presence of zero precipitation (the log-logistic distribution does not require such an operation)	
$H(x) = p + (1 - p)G(x)$, (8)	$H(x) = F(x)$. (9)
where p is probability of no precipitation.	
(4) Transformation of the cumulative probability into a standard normal variable and calculation of the rSPI or rSPEI	
$Z = \begin{cases} -z & \text{for } 0 < H(x) \le 0.5 \\ +z & \text{for } 0.5 < H(x) < 1 \end{cases}$, (10)	
where $z = t - (c_0 + c_1 t + c_2 t^2)/(1 + d_1 t + d_2 t^2 + d_3 t^3)$, (11)	
with $t = \begin{cases} \sqrt{-2\ln(H(x))} & \text{for } 0 < H(x) \le 0.5 \\ \sqrt{-2\ln(1 - H(x))} & \text{for } 0.5 < H(x) \le 1 \end{cases}$, (12)	
and approximation coefficients as: $c_0 = 2.515517$, $c_1 = 0.802853$, $c_2 = 0.010328$, $d_1 = 1.432788$, $d_2 = 0.189269$, $d_3 = 0.001308$ and Z is represented for rSPI or rSPEI.	
(5) Calculation of drought intensity by dividing the drought severity by the drought duration	
$S = \frac{\sum_{i=1}^{T} (\mathrm{rSPI}_i / \mathrm{rSPEI}_i - K)}{T}$, (13)	

(Continues)

TABLE 2 (Continued)

rSPI	rSPEI
where S is the drought intensity, K is the drought threshold, and T is the drought duration.	
(6) Calculation of drought frequency by dividing the number of droughts (n) by the time period (*N*)	
$P=\frac{n^*}{N}100\%$. (14)	
(7) Calculation of the probability of an rSPEI drought episode occurring during an rSPI drought episode	
$Cp(\text{rSPEI})=\frac{T_{\text{rSPEI}\mid\text{rSPI}}}{T_{\text{rSPI}}}$, (15)	
where $T_{\text{rSPEI/rSPI}}$ is the duration of rSPEI within rSPI, and T_{rSPI} is the duration of rSPI drought episodes at a certain station over time.	
(8) Calculation of trend using the Mann–Kendall test statistic (S)	
$S=\sum_{i=1}^{n-1}\sum_{j=i+1}^{n}\text{sgn}(x_j-x_i)=\begin{cases}1 & (x_j-x_i)>0\\ 0 & (x_j-x_i)=0,\\ -1 & (x_j-x_i)<0\end{cases}$ (16)	
where n is the number of observations. For independent and randomly ordered data for large n, the S statistics approximate a normal distribution with mean $E(S)=0$ and a variance equal to:	
$\text{var}(S)=\frac{n(n-1)(2n+5)\sum_{k=1}^{m}t_k(k)(k-1)(2k+5)}{18}$, (17)	
where n is the number of observations, m is the number of tied groups and t_k denotes the number of ties of extent k. Standardized test statistic Z was calculated using the equation:	
$Z=\begin{cases}\frac{S-1}{\sqrt{\text{var}(S)}} & \text{if } S>0\\ 0 & \text{if } S=0\\ \frac{S+1}{\sqrt{\text{var}(S)}} & \text{if } S<0\end{cases}$. (18)	
The null hypothesis of no trend is rejected if the absolute value of the Z statistic exceeds the critical value $Z\alpha$ at a chosen level of significance α.	
(9) Calculation of the modified Mann-Kendall test statistic to address autocorrelation issues	
$V^*(S)=V(S)\cdot\frac{n}{n^*}$, (19)	
where n is the actual sample size off sample data, n^* is the effective sample size and n/n^* is correction factor.	
$n^*=\frac{n}{1+2\cdot\frac{\rho_1^{n+1}-n\cdot\rho_1^2+(n-1)\cdot\rho_1}{n(\rho_1-1)^2}}$. (20)	
(10) Calculation of the magnitude of the Mann–Kendal trend	
$\beta=\text{Median}\left(\frac{X_j-X_i}{j-i}\right)$, (21)	
where β is Sen's slope estimator, and X_j and X_i are data values at times j and i ($j>i$).	

key drivers of drought intensity and frequency at different time scales (Jolliffe & Cadima, 2016). Data were standardized to a standard deviation of 1, followed by a varimax rotation to increase factor independence and maximize explained variance. The Kaiser criterion, with eigenvalues greater than 1, was used to determine the optimal number of extracted factors. Relationships between variables were interpreted as strong (≥0.75) or moderate (≥0.50 and <0.75). The versatility of PCA in climate research, including the assessment of drought, has been demonstrated in several studies (e.g., Tadić et al., 2019; Ventura et al., 2023; Xie et al., 2013).

3 | RESULTS

3.1 | Spatial pattern of drought across the orographic barrier

Analysis of the drought intensity and frequency reveals the annual spatial pattern of drought (Figure 3). rSPI drought intensity ranges from 0.3 to 0.6 over all time scales, with the highest values at elevated stations and a maximum at Cherrapunji. rSPEI drought intensity has a wider range of 0.3–1.0. Notably, drought intensity increases from the south (windward) to the north (leeward) across the orographic barrier, with Gauhati

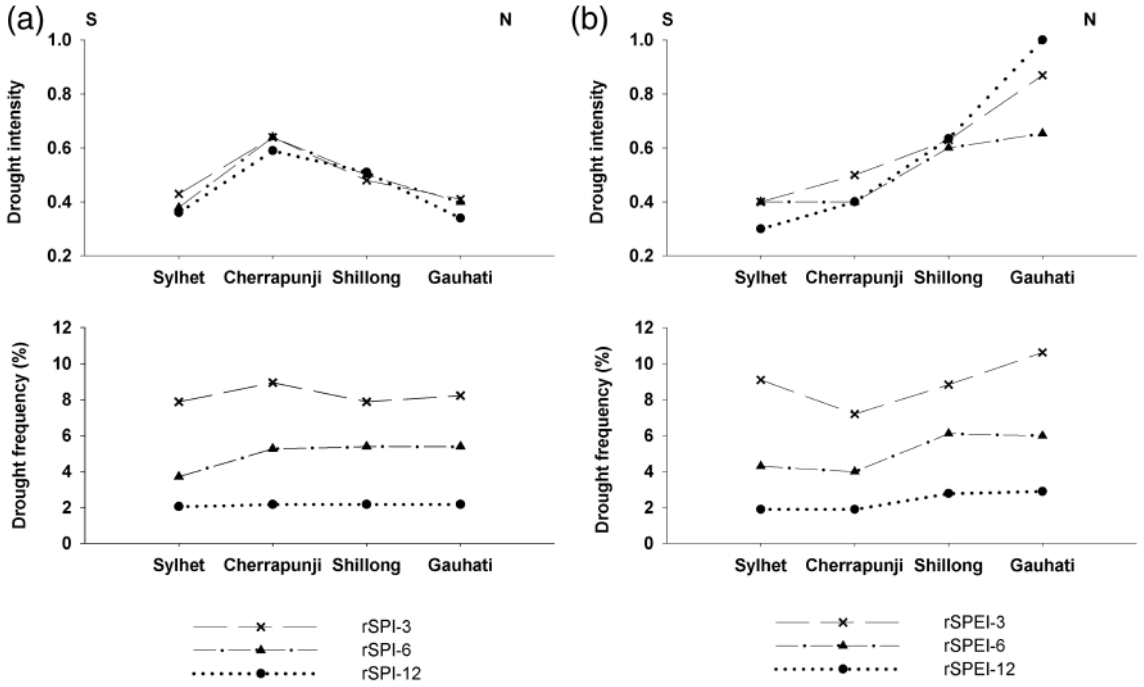

FIGURE 3 Distribution of annual drought intensity and frequency of (a) rSPI and (b) rSPEI across the orographic barrier on different time scales.

exhibiting the highest values. However, this parameter does not present distinct spatial variations for both indices on different time scales.

The overall frequency of droughts is similar between rSPI and rSPEI, ranging from 2% to 11% per year. Their spatial distribution shows some variation, but the differences between stations remain within 2%–3%. Cherrapunji has the highest rSPI drought frequency on a 3-month time scale. However, as the time scale increases, the spatial differences decrease, resulting in a drought frequency of 2% for rSPI-12 over the entire study area. Conversely, for rSPEI, the 3- and 6-month time scales give the lowest drought frequency at Cherrapunji. Other stations, particularly Gauhati on the leeward side of the orographic barrier, experience higher rSPEI drought frequencies. As the time scale increases, the differences in drought frequency also decrease, with rSPEI-12 ranging from 2% to 3% annually.

Analysing drought intensity and frequency in different seasons provides insight into their contribution to the annual pattern across the orographic barrier. The range of variation in rSPI drought intensity over the four seasons is slightly wider (0.3–0.8) than that of the annual pattern (Figure 4). In contrast, the seasonal ranges of rSPI drought intensity do not differ from those of the whole year. The lowest rSPI drought intensity occurs during the monsoon season, while rSPEI shows consistent ranges of drought intensity in all seasons. The patterns of drought intensity are more similar in two pairs of seasons: winter–pre-monsoon and monsoon–post-monsoon.

The spatial distribution of drought frequency for both rSPI and rSPEI in different seasons reflects their annual patterns (Figure 5). However, the drought frequency values exhibit a much wider seasonal range of variation (5%–30%) compared to the annual values (2%–11%). In addition, drought frequency tends to be generally lower for rSPI than for rSPEI. With increasing time scales, the spatial differences in drought frequency across the orographic barrier decrease for both indices. Specifically, over the 12-month time scale, the entire study area has a drought frequency of 5%–15% in all seasons. The highest and lowest drought frequencies for both indices occur during the winter and monsoon seasons, respectively. Remarkably, the patterns of drought intensity show a higher degree of similarity in two pairs of seasons: winter–pre-monsoon and monsoon–post-monsoon.

3.2 | Temporal pattern of drought across the orographic barrier

The modified M–K test indicated negative trends in rSPI for most stations over all time scales except Sylhet and Gauhati over the 6-month scale (Table 3). None of the stations showed statistically significant trends in rSPI. As rSPEI incorporates evapotranspiration, it therefore differs from

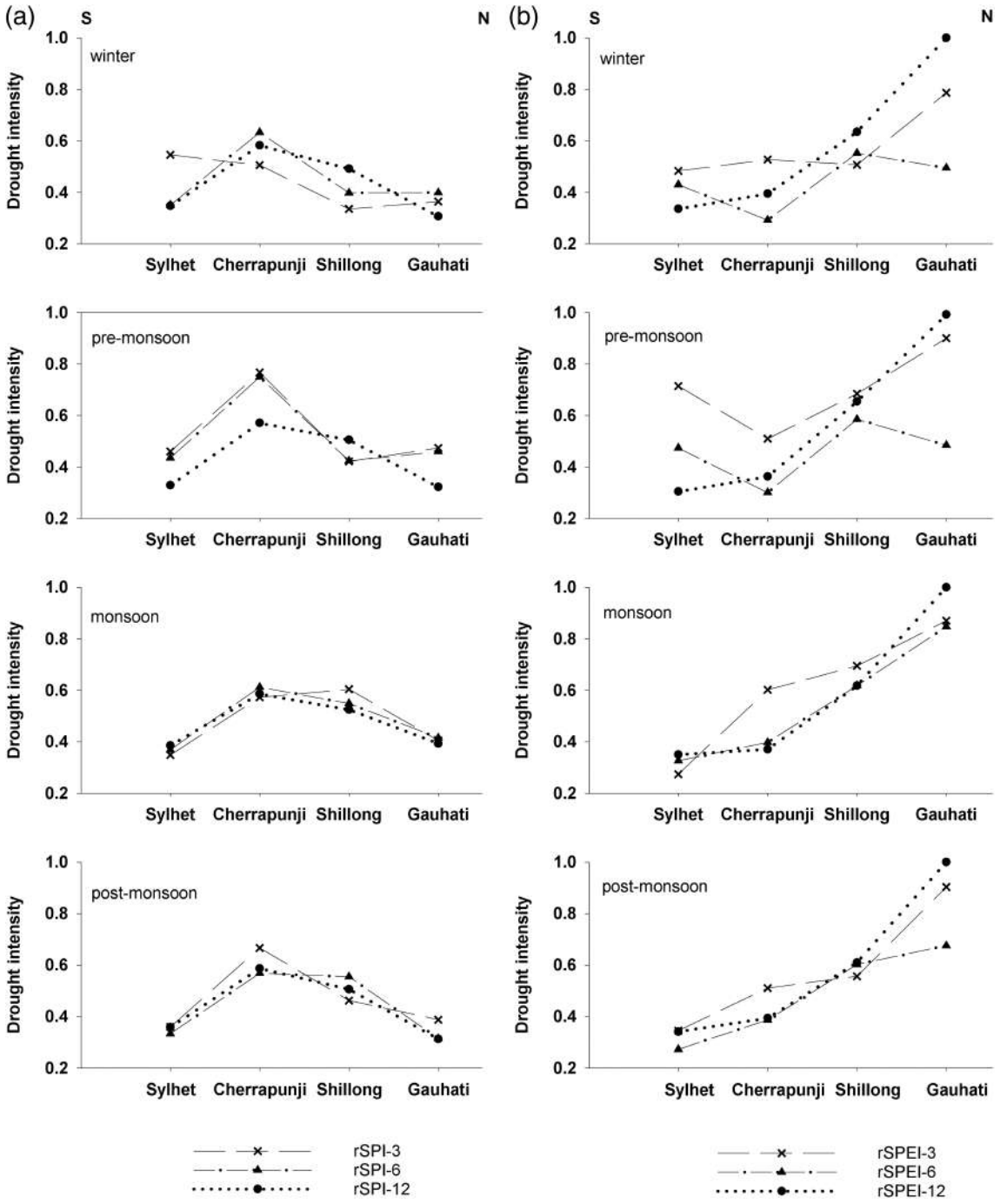

FIGURE 4 Distribution of seasonal drought intensity of (a) rSPI and (b) rSPEI across the orographic barrier on different time scales.

rSPI. The rSPEI trends are negative except in Sylhet, but all are statistically insignificant. In a broader sense, the Sylhet station exhibits the narrowest range of trend variation in both indices across the three time scales (0.0000–0.0031 year^{-1}), while the Cherrapunji and Gauhati stations demonstrate the widest trend range (−0.0004 to −0.0066 and 0.0010 to −0.0125 year^{-1}, respectively).

The temporal analysis of drought indicates that extending the time scale from 3 to 6 and 12 months reduces the frequency of drought while increasing its duration (Figure 6). In addition, the rSPI values indicate an increased number of intense drought episodes at the higher elevated stations of Cherrapunji and Shillong. Conversely, the rSPEI values indicate intensified drought episodes at leeward stations such as Shillong and Gauhati. Over longer time scales, particularly the 12-month intervals, drought episodes indicated by both indices coincide with below-mean annual rainfall for the Assam

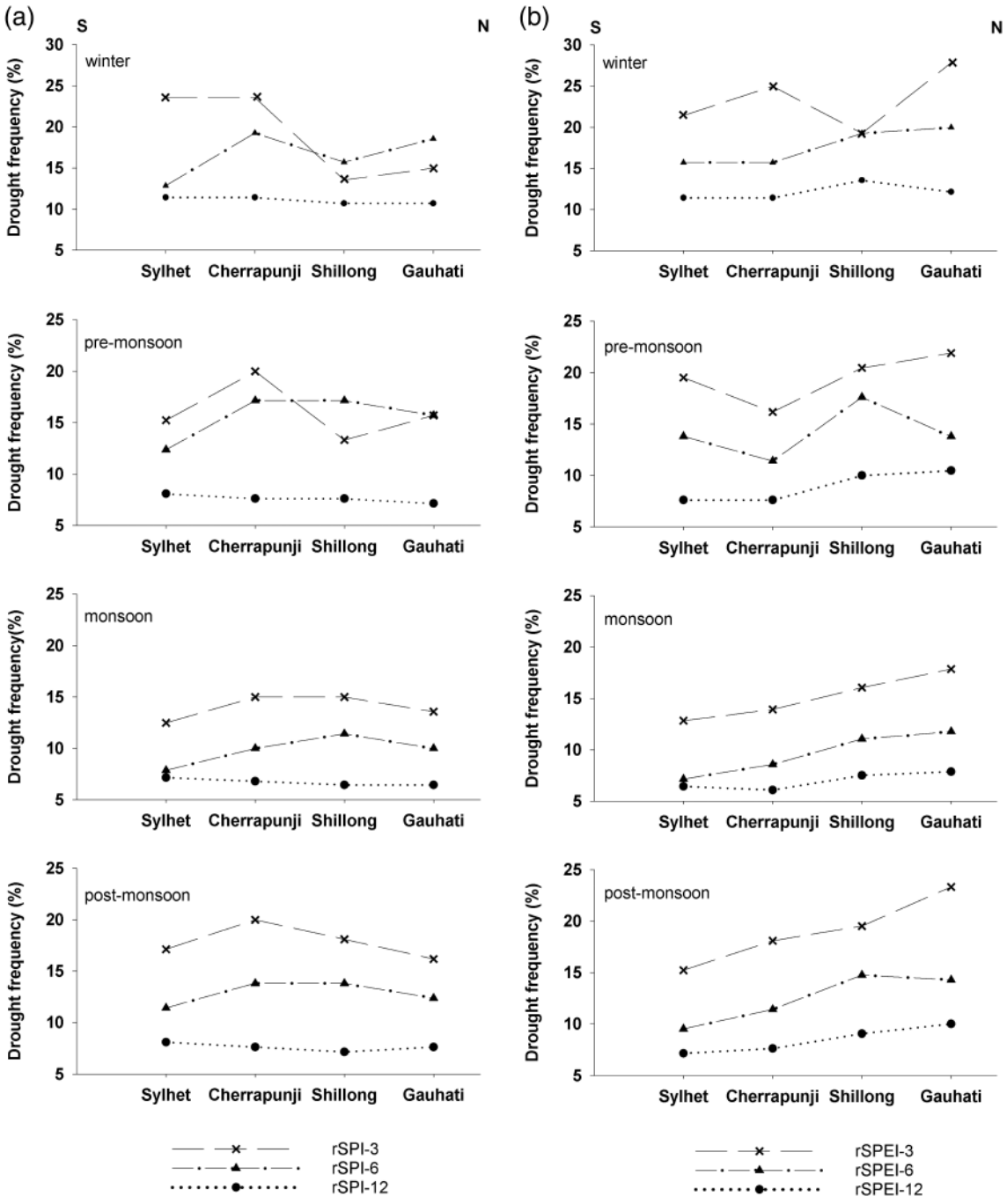

FIGURE 5 Distribution of seasonal drought frequency of (a) rSPI and (b) rSPEI across the orographic barrier on different time scales.

and Meghalaya Meteorological Subdivision. The rainfall trend for the subdivision is negative overall but not statistically significant ($Z = -1.4398$, $p = 0.1499$). Two periods of increased drought frequency are evident: the 1960s and 1970s and since the mid-2000s. These periods were interrupted by wetter years in the 1990s. The driest years (those with rainfall deviations greater than one standard deviation) were 1962, 1967, 2006, 2009 and 2018. Clusters of such dry years also occurred around the transition from the 1970s to the 1980s and at the beginning of the second decade of the 21st century.

3.3 | Effectiveness of relative drought indices in delineating drought across the orographic barrier: Conceptual model

Through analyses of the rSPI and rSPEI of drought intensity and frequency over three time scales from 1951 to

TABLE 3 Coefficients of the modified M–K trend test and significance coefficients (p) of rSPI and rSPEI at stations located across the orographic barrier in northeastern India and Bangladesh over different time scales during 1951–2020.

Station	rSPI	Trend (year^{-1})	Z	p-value	rSPEI	Trend (year^{-1})	Z	p-value
Sylhet	rSPI-3	0.0023	−0.10	0.46	rSPEI-3	0.0000	−0.13	0.45
	rSPI-6	0.0030	0.04	0.52	rSPEI-6	0.0006	0.03	0.51
	rSPI-12	0.0031	0.03	0.51	rSPEI-12	0.0001	0.03	0.51
Cherrapunji	rSPI-3	−0.0004	−0.50	0.31	rSPEI-3	−0.0028	−0.55	0.29
	rSPI-6	−0.0028	−0.32	0.37	rSPEI-6	−0.0028	−0.32	0.37
	rSPI-12	−0.0066	−0.52	0.30	rSPEI-12	−0.0055	−0.53	0.30
Shillong	rSPI-3	−0.0016	−0.46	0.32	rSPEI-3	−0.0026	−0.61	0.27
	rSPI-6	−0.0019	−0.22	0.41	rSPEI-6	−0.0031	−0.23	0.41
	rSPI-12	−0.0002	−0.16	0.44	rSPEI-12	−0.0022	−0.16	0.44
Gauhati	rSPI-3	−0.0005	−0.93	0.18	rSPEI-3	−0.0054	−0.92	0.18
	rSPI-6	0.0010	−0.55	0.29	rSPEI-6	−0.0042	−0.54	0.29
	rSPI-12	−0.0017	−0.63	0.27	rSPEI-12	−0.0125	−0.64	0.26

Note: No significant test results were obtained.

2020, a model has been developed that outlines the impact of the orographic barrier on the spatial variation of rSPI and rSPEI droughts (Figure 7). It presents the effectiveness of relative drought indices in delineating drought characteristics within complex topographies. The model highlights two consistent features, irrespective of drought timescale. The first feature is the spatial divergence of drought intensity and frequency between stations within the same index. The second feature is the spatial differentiation of droughts identified by the two drought indices. This differentiation is evident in the shift of the maximum drought occurrence from the crest of the orographic barrier to its leeward side between the rSPI and rSPEI indices. In particular, the smallest differences in drought parameters between rSPI and rSPEI are observed in the foreland of the orographic barrier.

Differences in drought characteristics prompt an investigation of the predictive potential of rSPI in relation to rSPEI drought occurrence. Calculated conditional probabilities (Cp) shed light on this relationship, capturing the influence of prior rainfall information embedded in rSPI on the likelihood of rSPEI drought, taking into account both rainfall and evapotranspiration. The calculated Cp values for drought episodes show a clear correlation with increasing annual rainfall over all time scales, as shown in Table 4. The Gauhati and Cherrapunji stations, which have the lowest and highest annual rainfall, respectively, have Cp values ranging from 0.46 to 1.00. The Sylhet and Shillong stations, which receive moderate annual rainfall, occupy intermediate positions within this spectrum. Over the longest time scale of 12 months, the Cp differences between the windward stations of Sylhet and Cherrapunji almost disappear.

Considerable differences in annual rainfall between stations result in PET contributing only 8% to total annual rainfall at Cherrapunji and a remarkable 71% at Gauhati. This divergence leads to the almost simultaneous occurrence of drought episodes identified by rSPI and rSPEI at Cherrapunji, highlighted by the highest Cp value. Conversely, the substantial PET contribution to annual rainfall in Gauhati suggests a greater likelihood of decoupled drought episodes between rSPI and rSPEI, as indicated by the lowest Cp value.

3.4 | Major drivers of drought

Although droughts vary in intensity and frequency over different time scales, their main drivers are rooted in common meteorological variables. They represent a complex interplay between rainfall and temperature (as indicated by PET), with variability in both leading to a lack of rainfall and the development of drought. The rainfall only rSPI and its variant rSPEI, which includes both rainfall and PET, can capture droughts associated with increased water demand due to evaporation and transpiration. It remains unclear, however, which of these variables primarily drive the spatiotemporal evolution of drought, and what role elevation plays in the complex topography. Furthermore, the key drivers may differ between rSPI and rSPEI, as well as between different drought parameters such as intensity and frequency. To investigate this aspect, a PCA analysis was performed considering rSPI and rSPEI drought intensity and frequency over all time scales, as well as rainfall and PET and their coefficients of variation and elevations.

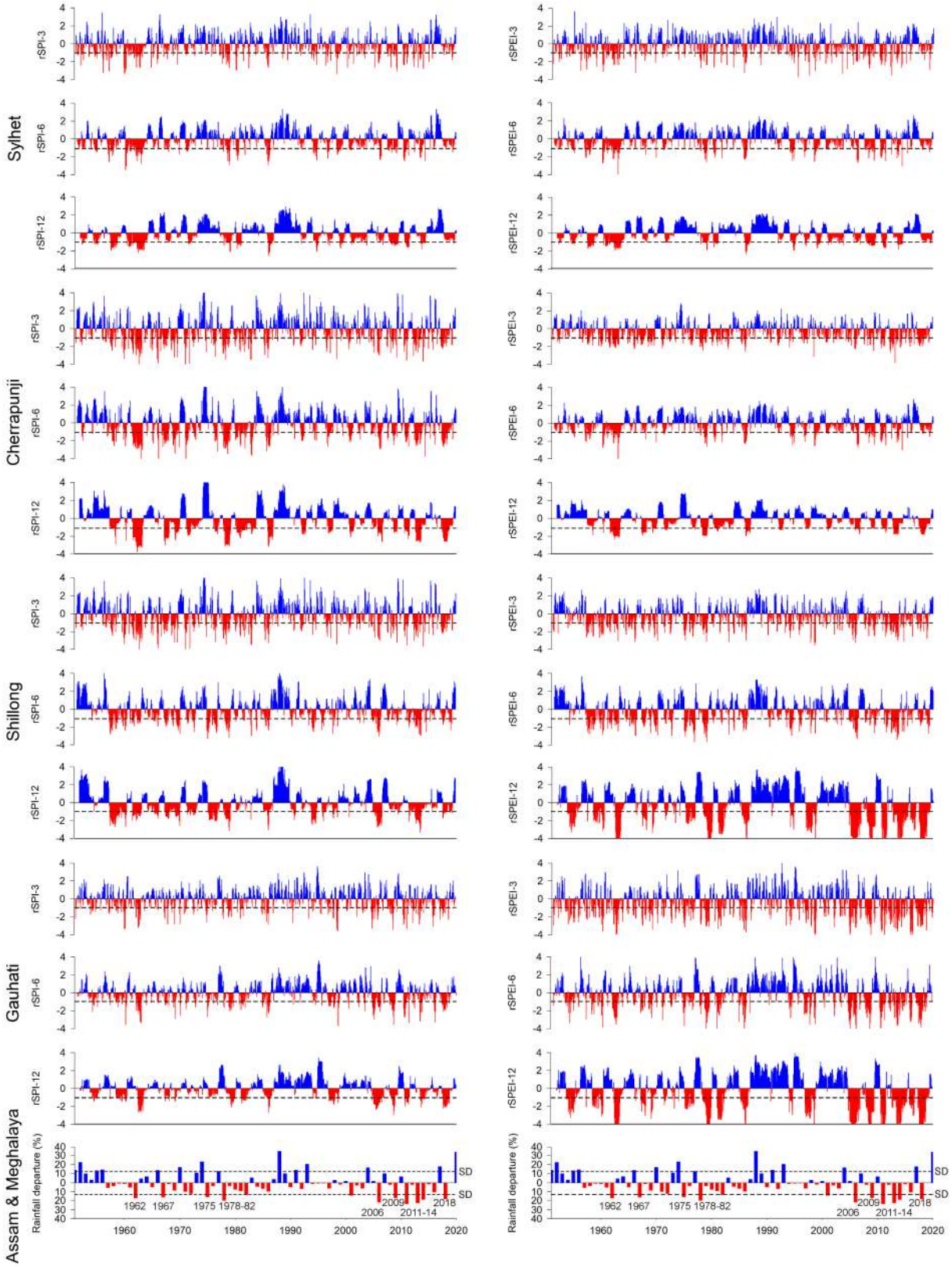

FIGURE 6 The SPI and SPEI across the orographic barrier on different time scales and annual rainfall departure for Assam & Meghalaya Meteorological Subdivision. Blue colour—wet period, red colour—dry period, dashed line—drought boundary, SD—standard deviation from mean annual rainfall for Assam and Meghalaya Meteorological Subdivision. [Colour figure can be viewed at wileyonlinelibrary.com]

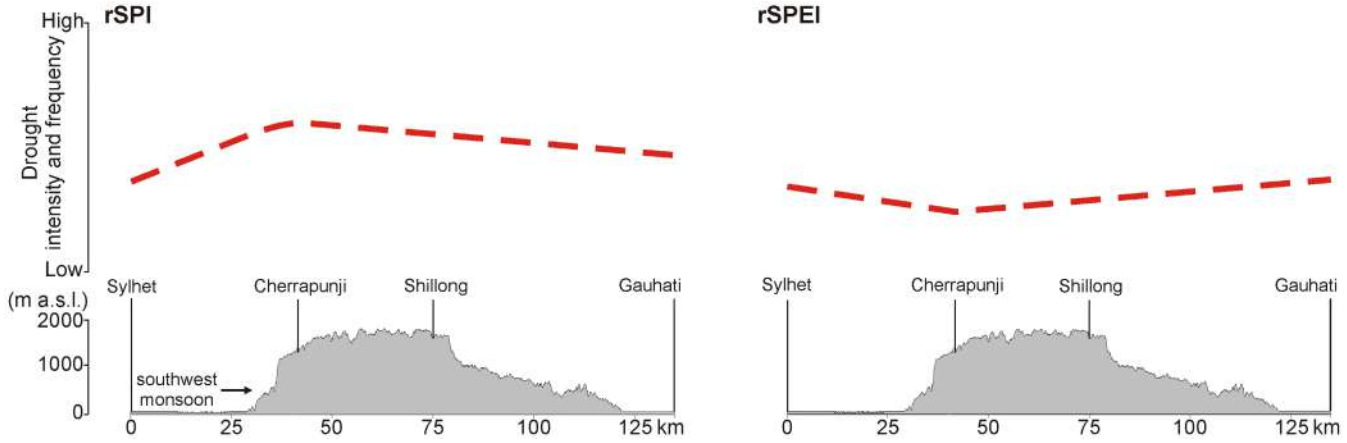

FIGURE 7 Conceptual model of the occurrence of (a) rSPI and (b) rSPEI drought intensity and frequency across the orographic barrier over all time scales. [Colour figure can be viewed at wileyonlinelibrary.com]

Cp	Sylhet	Cherrapunji	Shillong	Gauhati
Cp(rSPEI-3|rSPI-3)	0.66	0.90	0.71	0.56
Cp(rSPEI-6|rSPI-6)	0.91	1.00	0.87	0.68
Cp(rSPEI-12|rSPI-12)	0.99	1.00	0.82	0.46

TABLE 4 Conditional probability of an rSPEI drought episode occurring during an rSPI drought episode at stations across the orographic barrier at different time scales.

PCA effectively condensed the data set of rSPI and rSPEI drought intensity across all time scales into three factors, accounting for 99.9% of the variance (Figure 8a and Table 5). The first PCA factor shows a robust positive correlation between rSPI drought intensity, rainfall coefficient of variation and elevation, and a moderate association with annual rainfall. This correlation is reinforced by a stronger linear relationship between rSPI drought intensity and rainfall coefficient of variation ($R^2 = 0.9351$), which exceeds the correlations with annual rainfall ($R^2 = 0.6556$) and elevation ($R^2 = 0.6214$) at all time scales. The highest coefficients of variation for annual rainfall correspond to higher-elevation stations, lower values correspond to stations in the foreland and hinterland on the leeward side of the orographic barrier. The second PCA factor reveals a moderate association between rSPEI drought intensity and PET coefficient of variation, coupled with a moderate association with annual rainfall. This relationship is underlined by the strongest linear correlation between rSPEI and PET coefficient of variation ($R^2 = 0.4115$), surpassing the correlation with rainfall ($R^2 = 0.3046$). In general, the stations at the lowest elevations have the highest PET values, while the annual PET coefficients of variation increase progressively from south to north across the orographic barrier. The third factor indicates a moderate relationship between the PET coefficient of variation and elevation.

The PCA reduced the rSPI and rSPEI drought frequency dataset into three factors, which together explain 99.9% of the variance (Figure 8b and Table 5). The first factor of the PCA shows a consistently strong relationship between rSPI and rSPEI drought frequency, together with a moderate relationship with the PET coefficient of variation at all time scales. The second factor demonstrates that only rSPI-3 drought frequency correlates with PET, with a negative association with elevation and annual rainfall coefficient of variation. The third factor shows a moderate negative correlation of rSPEI-6 with rainfall. In contrast to drought intensity, the linear correlations of drought frequency for both indices with other variables such as rainfall, PET, their coefficients of variation and elevation are comparatively lower, typically ranging between $R^2 = 0.2$ and 0.7 for individual time scales of 3, 6 and 12 months.

4 | DISCUSSION

4.1 | Differences in spatial drought characteristics revealed by rSPI and rSPEI

This study examined the impact of the orographic barrier on drought characteristics in the highest global rainfall region using relative drought indices from 1951 to 2020. It exploits the significant climatic variation across the orographic barrier to demonstrate its influence on local-scale drought characteristics at the station level. At the same time, the selected stations represent larger,

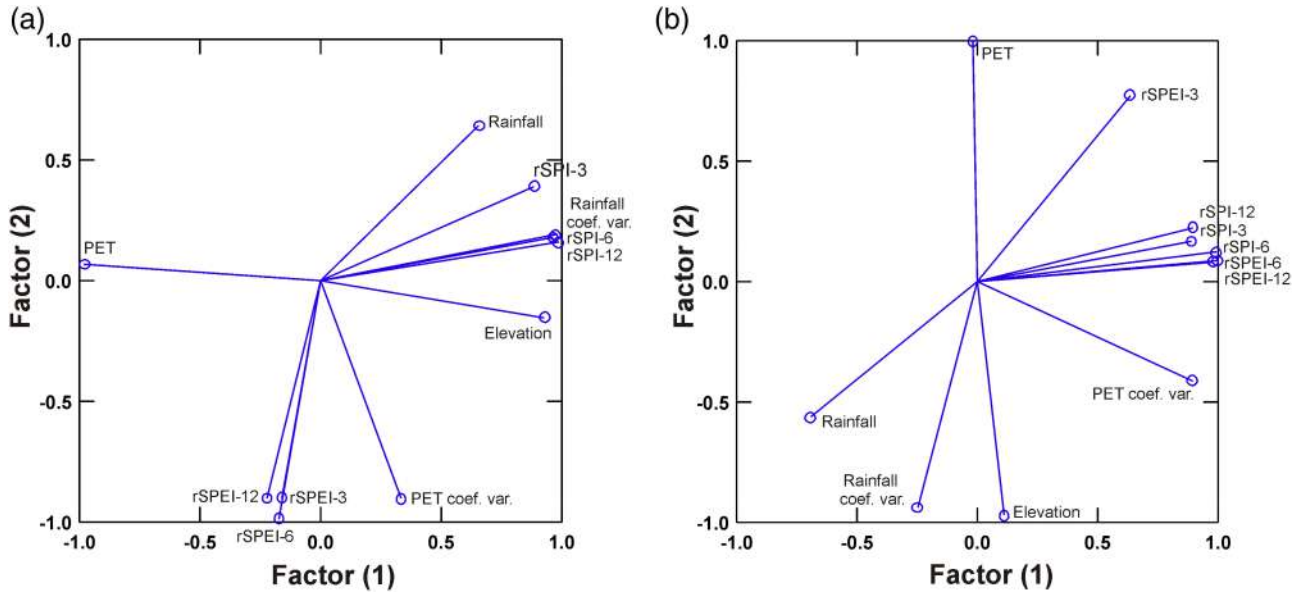

FIGURE 8 The first two factors of PCA analyses. (a) Drought intensity and (b) drought frequency of the rSPI and rSPEI indices on all time scales. [Colour figure can be viewed at wileyonlinelibrary.com]

TABLE 5 Varimax rotated factor loading matrix from PCA for rSPI and rSPEI intensity and frequency at four stations across the orographic barrier.

	rSPI and rSPEI intensity			rSPI and rSPEI frequency		
Variable	**Factor 1**	**Factor 2**	**Factor 3**	**Factor 1**	**Factor 2**	**Factor 3**
rSPI-3	**0.943**			**0.987**		
rSPI-6	**0.994**			**0.910**		
rSPI-12	**0.964**			**0.976**		
rSPEI-3		**−0.989**		0.578	0.735	
rSPEI-6		**−0.906**		**0.801**		0.599
rSPEI-12		**−0.977**		**0.894**		
Rainfall	**0.765**					**−0.760**
Rainfall coef. variation	**0.991**				**−0.895**	
PET	**−0.916**				**0.999**	
PET coef. variation		−0.710	−0.673	0.723		
Elevation	**0.833**		−0.554		**−0.992**	
Cumulative variance (%)	55.2	87.6	99.9	47.8	82.8	99.9

Note: Strong correlations (≥0.75) are indicated in bold type, and moderate loadings (≥0.50 and <0.75) are indicated in normal type.

relatively uniform areas in terms of topography and climatic conditions.

The application of run theory reveals distinct drought characteristics between the rSPI and rSPEI indices, providing the basis for constructing a conceptual model of drought patterns across the orographic barrier (Figures 3 and 7). The rSPI index highlights increased drought intensity and frequency at elevated stations, particularly Cherrapunji, where the difference in elevation between the Bengal Plain and the southern edge of the Meghalaya Plateau is greatest. This underscores the important role of elevation in shaping the amount and variability of rainfall, which ultimately affects the intensity and the frequency of droughts, as indicated by the rSPI index. Various studies conducted across terrain barriers have highlighted the profound influence of topography on the amount and intensity of orographic monsoonal rainfall (Anders et al., 2006; Goswami et al., 2010; Prokop &

Walanus, 2017; Tawde & Singh, 2015). The key topographic parameters in this influence are the length and width of the mountain barrier, followed by the steepness of the windward slope and elevation. Essentially, a larger barrier size results in more effective enhancement and greater intensity of rainfall.

The Meghalaya Plateau which is 300 km long and 100 km wide, has a nearly vertical southern wall that reaches elevation in the range of 1300–1400 m a.s.l. in some areas. The vast plateau is able to spatially block the incoming moisture flux from the Bay of Bengal, resulting in condensation (Ahmed et al., 2022; Kirshbaum & Smith, 2008). The location of Cherrapunji within a typical inland tropical mountain condensation zone further exacerbates rainfall variability (Bruijnzeel, 2001; Sato, 2013), resulting in the rSPI indicating drought even during the peak monsoon. The Shillong station, located at the edge of the influence of this condensation layer, and especially Gauhati, located in the rain shadow on the leeward side, experience lower rainfall and less variability. Consequently, the spatial distribution of droughts, as indicated by the rSPI based on rainfall alone, largely reflects their spatial distribution and variability both annually and in individual seasons.

Conversely, the rSPEI identifies more intense and frequent droughts at leeward stations, particularly Gauhati, which experiences the highest PET contribution to rainfall across all time scales. Gauhati's hinterland location on the leeward side of the orographic barrier, coupled with reduced monsoon rainfall and increased evapotranspiration, makes it particularly vulnerable to drought. This vulnerability is attributed to the influence of the extensive barrier formed by the Meghalaya Plateau, which reinforces the rain shadow effect on the leeward side (Damseaux et al., 2020; Paul & Maity, 2023).

Over longer time scales, the differences in drought frequency between stations decrease for both indices. On a 12-month scale, the local orographic climatic influence on drought frequency diminishes substantially for both indices, possibly because of the prevalence of more prolonged regional droughts covering larger areas (Mallya et al., 2016). This assessment extends and corroborates the overarching model, elucidating the interplay between the rSPI and rSPEI indices with respect to the influence of the orographic barrier.

4.2 | Limited effect of topography on rSPI and rSPEI trends

The influence of topography on the trends in rSPI and rSPEI was found to be limited. The absence of statistically significant negative trends in these drought indices over all time scales considered was true for all stations except for those at the foreland of the orographic barrier. This finding is consistent with previous analyses that confirmed the absence of significant trends in rainfall at all stations, as well as in the broader regions of northeastern India and Bangladesh (Bari et al., 2017; Kuttippurath et al., 2021; Prokop & Walanus, 2003; Shahid, 2010). Thus, the potential influence of topography on the temporal characteristics of drought at individual stations is overwhelmed by the monsoon circulation. Examination of the time span from 1951 to 2020 revealed a link between prolonged droughts and dry years in the Assam and Meghalaya Meteorological Subdivision. Instances of prolonged periods of slightly below-average annual rainfall, such as 1978–1982, corresponded to prolonged drought conditions. However, it is noteworthy that only three specific drought events in 1967, 2009 and 2018 coincided with droughts in peninsular India (Mishra, 2020a). This suggests that the majority of droughts in the study area are regional in scale and, similar to rainfall patterns, have weak correlations with the central Indian subcontinent and other regions of Bangladesh (Guhathakurta et al., 2017; Kamruzzaman et al., 2019; Mallya et al., 2016).

4.3 | Effect of rainfall and PET variability on seasonal rSPI and rSPEI drought characteristics across the orographic barrier

The PCA analysis results highlight the significant role of rainfall variability and PET variability in shaping rSPI and rSPEI drought intensity, respectively, across the orographic barrier (Figures 3 and 8). Given the dynamic variability of rainfall and evapotranspiration throughout the year (Krishnamurthy & Shukla, 2000; Prokop & Walanus, 2015), a deeper understanding of these contributors (drivers) to the spatiotemporal variability of droughts in the study area can be gained through an analysis of synoptic-scale seasonal climatic conditions.

During winter, the northeasterly winds carrying dry air masses from the interior of the Asian continent are more pronounced in the study area (Rajeevan et al., 2012). The gently sloping northern side of the Meghalaya Plateau presents less of an obstacle to these winds than the steeper southern plateau wall, resulting in reduced orographic effects. Atmospheric conditions in winter typically exhibit stable stratification with low moisture content, resulting in infrequent rainfall events (Mahanta et al., 2013). However, it is worth noting that in low rainfall seasons, small deviations from the mean can result in locally significant negative or positive values of the drought indices due to the

relatively small mean totals (Rouault & Richard, 2003). This notion is supported by the observed high coefficient of variation of rainfall, ranging from 106% in Gauhati to 160% in Cherrapunji for individual months. At the same time, the PET coefficient of variation shows a narrower range of variation, from 6% in Gauhati to 11% in Cherrapunji. As a result, there is significant spatial variation in drought intensity and frequency for both indices between three time scales within the same winter season across the orographic barrier (Figures 4 and 5). In particular, the distribution of rSPI-3 and rSPEI-3 differs from the distribution of both indices for the longer 6- and 12-month time scales.

During the pre-monsoon season, the study area receives a remarkable amount of rainfall compared to peninsular India (Kumar & Naidu, 2020), highlighting the important role of the elevated Meghalaya Plateau as an orographic barrier. South of this barrier, nor'westers, characterized by irregular severe thunderstorms from March to May, gain strength through interaction with the warm, moisture-laden air mass brought by the southern low-level jet from the Bay of Bengal (Das et al., 2015; Mahanta et al., 2013). Just north of the plateau, in the Brahmaputra Valley, a combination of abundant surface water from preceding rains and monsoon floods, together with an atmosphere conducive to convection, leads to localized conversion of moisture into rainfall (Ganguly et al., 2023). Consequently, irregular rainfall of different origin and timing, with coefficients of variation ranging from 36% in Sylhet to 122% in Cherrapunji for individual months, interspersed with dry periods with the highest PET of all seasons, collectively contribute to the remarkable spatial variability of both drought indices.

During the monsoon season, extensive stratiform and convective rainfall systems develop, locally enhanced by orographic uplift (Goswami et al., 2010; Romatschke et al., 2010; Romatschke & Houze, 2011). The combination of high rainfall, increased humidity, and cloud cover leads to a notable reduction in evapotranspiration. With the monsoon season exhibiting the lowest coefficient of variation of rainfall among the seasons (ranging from 30% in Sylhet to 57% in Shillong), along with consistent PET variability, both drought intensity and frequency decrease at all stations. Nevertheless, monsoon rainfall itself exhibits distinct submonthly quasi-bi-weekly and 30- to 60-day Madden–Julian oscillation periodicities (Fujinami et al., 2011, 2017; Murata et al., 2008; Sato, 2013). During phases of increased rainfall, moist southwesterly winds strike the southern slopes of the plateau, resulting in intense convective rainfall (accounting for 50%–70% of total rainfall). Conversely, during phases of reduced rainfall, a southeasterly wind bypasses the plateau, reducing convective rainfall over the southern slopes to a range of 30%–50%. These large convective rainfall systems are confined to a zone up to approximately 40 km wide in the southern part of the Meghalaya Plateau, encompassing the Cherrapunji and, less frequently, Shillong stations (Prokop & Walanus, 2015). Beyond this area, Gauhati in the Brahmaputra valley rarely experiences extreme rainfall. Consequently, sub-monthly rainfall variability, which influences monthly patterns across the orographic barrier (Murata et al., 2007, 2008), plays a crucial role in determining the spatial distribution of drought during the monsoon.

However, droughts in Cherrapunji between June and August should be interpreted cautiously. The average rainfall for these months is 2500 mm, with a range of 500–6700 mm between 1951 and 2020. Such large deviations from the mean indicate the potential for drought even in months with relatively high rainfall. In September, the last month of the monsoon season, minimal rainfall of just a few tens of millimetres can initiate a drought that persists throughout the remaining months.

In the post-monsoon season, the study area experiences relatively reduced rainfall due to the retreat of the ITCZ (Syroka & Toumi, 2004). This transition is characterized by a shift from more convective to less convective rainfall, combined with irregular tropical cyclone activity originating in the Bay of Bengal (Fahad et al., 2023; Romatschke et al., 2010; Romatschke & Houze, 2011). As a result, Cherrapunji experiences extreme rainfall from these cyclones, while the leeward stations receive comparatively less rainfall (Singh et al., 2011). As the post-monsoon season progresses from October to December, there is an escalation in the rainfall coefficient of variation at all stations, shifting from 60%–85% to 160%–200%. This increase in variability coincides with a consistent PET coefficient of variation from the previous season. These factors contribute to months with little or no rainfall at each station. Consequently, there is a slight increase in drought intensity and a considerable increase in drought frequency during the post-monsoon season, as indicated by both rSPI and rSPEI (Figures 4 and 5).

The similarity of the drought intensity and frequency patterns of both indices in the monsoon and post-monsoon seasons reflecting the annual pattern at all stations, underscores the significant influence of these two seasons on the overall annual drought pattern. This influence is closely linked to summer monsoon in the region, when approximately three-quarters of the total annual rainfall occurs (Ahmed & Karmakar, 1993; Pai et al., 2020). Throughout the other seasons, the inflow of moist southwesterly air from the Bay of Bengal remains a notable meteorological feature of the study area (Sahany et al., 2018). This feature is also evident in the localized rainfall enhancement due

to orographic uplift, resulting in relatively high but erratic rainfall patterns at the Cherrapunji station.

4.4 | Drought polices and plans

The rSPI and rSPEI show that drought vulnerability varies across the complex terrain of northeastern India and Bangladesh, requiring season-specific and locally tailored mitigation strategies. This is challenging given the year-round cultivation of crops such as rice, which requires a consistent water supply throughout the growing season (Luo et al., 2022).

Both relative indices indicate that northeastern Bangladesh is least prone to drought. In the rest of the area, the rSPEI better reflects the drought risk. The rSPEI-3 indicates that cropping in the northern part of the Meghalaya Plateau and in the Brahmaputra valley, which is in the rainfall shadow during the summer monsoon season, is vulnerable. The impact of droughts in this area can be mitigated by using shorter-growing, drought-resistant rice varieties and adjusting planting schedules to the onset of the monsoon (Kumar et al., 2023). During the dry season, effective measures can include integrating traditional irrigation systems, such as bamboo, to divert hill stream or spring water in Meghalaya, or the using of stone, bamboo, and mud to channel water from streams in Assam. These measures can be supplemented with modern rooftop water harvesting systems, farm ponds, check dams and tube wells (Devi, 2018). The adoption of integrated agricultural practices, including fisheries and agroforestry, would further enhance the drought resilience of the entire region.

The limited and nonexistent spatial variation in rSPEI-6 and rSPEI-12, respectively, supports their usefulness in monitoring regional hydrological droughts, which are particularly important in northern Bangladesh. Here, intensive groundwater use for irrigation during droughts may impede the recharging of the water table during the monsoon and reduce water availability for agriculture during the dry season.

5 | CONCLUSIONS

In this study, we examined the impact of the orographic barrier in the border region between India and Bangladesh on drought characteristics. We used two relative drought indices over different time scales and analysed 70 years of climatic data collected in northeastern India and Bangladesh. Our results indicate following:

1. In the rainiest region of the world, droughts extend beyond the confines of the dry season inherent in the monsoon regime. These droughts manifest themselves across seasons and different spatiotemporal scales and usually have a regional character, with weak correlations with the rest of the Indian subcontinent and other parts of Bangladesh.
2. Among the spatial parameters considered, the orographic barrier had a stronger influence on drought intensity than on drought frequency. The rSPI index, which depends solely on rainfall, may overestimate drought frequency in areas with both high rainfall amounts and high rainfall variability. In this context, the rSPEI index, which depends on both rainfall and PET, appears to be better suited to capturing the nuanced spatial variation of drought within complex topographies.
3. The orographic barrier had minimal influence on the temporal distribution of rSPI and rSPEI, with statistically insignificant and mostly negative values reflecting similar trends in the rainfall datasets. Thus, the potential influence of topography on the temporal characteristics of drought at individual stations is overwhelmed by the monsoon circulation.
4. PCA and linear correlations show that the rainfall coefficient of variation and elevation play dominant roles in determining rSPI, whereas rSPEI is substantially influenced by the coefficient of variation of PET.

It is also important to recognize the limitations of examining the differential effects of drought, particularly as the stations analysed span the orographic barrier with the greatest difference in elevation. Consequently, contrasts in drought conditions between the lowlands and the plateau may be less pronounced, especially in the western part of the orographic barrier, which is lower in elevation. The study area exhibits considerable variation in geology, soils, land use and irrigation systems, particularly between the hilly plateau and the surrounding lowlands. The interplay of these natural and anthropogenic factors can influence rainfall and evapotranspiration patterns, potentially amplifying or mitigating drought impacts at the local level. The generalization of these results to regions with orographic barriers in non-monsoon climates may also require some adjustments.

AUTHOR CONTRIBUTIONS

Paweł Prokop: Conceptualization; writing – original draft; methodology; visualization; formal analysis. **Adam Walanus:** Conceptualization; writing – original draft; methodology; visualization; formal analysis.

ACKNOWLEDGEMENTS

This paper is the outcome of the cooperation between the Indian National Science Academy and Polish Academy of Sciences.

DATA AVAILABILITY STATEMENT

The data that support the findings of this study are available from the corresponding author upon reasonable request.

ORCID

Paweł Prokop https://orcid.org/0000-0002-1165-2499

REFERENCES

Acharya, N., Singh, A., Mohanty, U.C., Nair, A. & Chattopadhyay, S. (2013) Performance of general circulation models and their ensembles for the prediction of drought indices over India during summer monsoon. *Natural Hazards*, 66(2), 851–871. Available from: https://doi.org/10.1007/s11069-012-0531-8

Ahmed, R. & Karmakar, S. (1993) Arrival and withdrawal dates of the summer monsoon in Bangladesh. *International Journal of Climatology*, 13(7), 727–740. Available from: https://doi.org/10.1002/joc.3370130703

Ahmed, T., Lee, J., Jin, H.G. & Baik, J.J. (2022) Processes associated with extremely heavy precipitation in the Meghalaya Plateau region: a case modelling study. *Quarterly Journal of the Royal Meteorological Society*, 148(744), 1057–1074. Available from: https://doi.org/10.1002/qj.4246

Alam, M.M., Hossain, A.M. & Shafee, S. (2003) Frequency of Bay of Bengal cyclonic storms and depressions crossing different coastal zones. *International Journal of Climatology*, 23(9), 1119–1125. Available from: https://doi.org/10.1002/joc.927

Alamgir, M., Mohsenipour, M., Homsi, R., Wang, X., Shahid, S., Shiru, M.S. et al. (2019) Parametric assessment of seasonal drought risk to crop production in Bangladesh. *Sustainability*, 11(5), 1442. Available from: https://doi.org/10.3390/su11051442

Alamgir, M., Shahid, S., Hazarika, M.K., Nashrrullah, S., Harun, S.B. & Shamsudin, S. (2015) Analysis of meteorological drought pattern during different climatic and cropping seasons in Bangladesh. *Journal of the American Water Resources Association*, 51(3), 794–806. Available from: https://doi.org/10.1111/jawr.12276

Allen, R.G., Pereira, L.S., Raes, D. & Smith, M. (1998) *Crop evapotranspiration—guidelines for computing crop water requirements. FAO irrigation and drainage paper 56*. Rome: FAO.

Anders, A.M., Roe, G.H., Halle, B., Montgomery, D.R., Finnegan, N.J. & Putkonen, J. (2006) Spatial patterns of precipitation and topography in the Himalaya. *Geological Society of America Special Papers*, 398, 39–53.

Bari, S.H., Hussain, M.M. & Husna, N.E.A. (2017) Rainfall variability and seasonality in northern Bangladesh. *Theoretical and Applied Climatology*, 129, 995–1001. Available from: https://doi.org/10.1007/s00704-016-1823-9

Beguería, S., Vicente-Serrano, S.M., Reig, F. & Latorre, B. (2014) Standardized precipitation evapotranspiration index (SPEI) revisited: parameter fitting, evapotranspiration models, tools, datasets and drought monitoring. *International Journal of Climatology*, 34(10), 3001–3023. Available from: https://doi.org/10.1002/joc.3887

Bookhagen, B. & Burbank, D.W. (2006) Topography, relief, and TRMM-derived rainfall variations along the Himalaya. *Geophysical Research Letters*, 33(8), L08405. Available from: https://doi.org/10.1029/2006GL026037

Bruijnzeel, L.A. (2001) Hydrology of tropical montane cloud forests: a reassessment. *Land Use and Water Resources Research*, 1, 1–18. Available from: https://doi.org/10.22004/ag.econ.47849

Chandrasekara, S.S., Kwon, H.H., Vithanage, M., Obeysekera, J. & Kim, T.W. (2021) Drought in South Asia: a review of drought assessment and prediction in South Asian countries. *Atmosphere*, 12(3), 369. Available from: https://doi.org/10.3390/atmos12030369

Chao, W.C. (2012) Correction of excessive precipitation over steep and high mountains in a GCM. *Journal of the Atmospheric Sciences*, 69(5), 1547–1561. Available from: https://doi.org/10.1175/JAS-D-11-0216.1

Choudhury, B.A., Rajesh, P.V., Zahan, Y. & Goswami, B.N. (2021) Evolution of the Indian summer monsoon rainfall simulations from CMIP3 to CMIP6 models. *Climate Dynamics*, 58, 2637–2662. Available from: https://doi.org/10.1007/s00382-021-06023-0

Damseaux, A., Fettweis, X., Lambert, M. & Cornet, Y. (2020) Representation of the rain shadow effect in Patagonia using an orographic-derived regional climate model. *International Journal of Climatology*, 40(3), 1769–1783. Available from: https://doi.org/10.1002/joc.6300

Das, P.K., Dutta, D., Sharma, J.R. & Dadhwal, V.K. (2016) Trends and behaviour of meteorological drought (1901–2008) over Indian region using standardized precipitation–evapotranspiration index. *International Journal of Climatology*, 36(2), 909–916. Available from: https://doi.org/10.1002/joc.4392

Das, S., Sarkar, A., Das, M.K., Rahman, M.M. & Islam, M.N. (2015) Composite characteristics of Nor'westers based on observations and simulations. *Atmospheric Research*, 158–159, 158–178. Available from: https://doi.org/10.1016/j.atmosres.2015.02.009

Devi, C.V. (2018) Participatory management of irrigation system in north eastern region of India. *International Journal of Rural Management*, 14(1), 69–79. Available from: https://doi.org/10.1177/09730052187655

Dey, A., Chattopadhyay, R., Joseph, S., Kaur, M., Mandal, R., Phani, R. et al. (2022) The intraseasonal fluctuation of Indian summer monsoon rainfall and its relation with monsoon intraseasonal oscillation (MISO) and Madden Julian oscillation (MJO). *Theoretical and Applied Climatology*, 148(1–2), 819–831. Available from: https://doi.org/10.1007/s00704-022-03970-4

Dubrovsky, M., Svoboda, M.D., Trnka, M., Hayes, M.J., Wilhite, D.A., Zalud, Z. et al. (2009) Application of relative drought indices in assessing climate-change impacts on drought conditions in Czechia. *Theoretical and Applied Climatology*, 96, 155–171. Available from: https://doi.org/10.1007/s00704-008-0020-x

Fahad, A.A., Reale, O., Molod, A., Sany, T.A., Ahammad, M.T. & Menemenlis, D. (2023) The role of tropical easterly jet on the Bay of Bengal's tropical cyclones: observed climatology and

future projection. *Journal of Climate*, 36, 5825–5840. Available from: https://doi.org/10.1175/JCLI-D-22-0804.1

Fahad, A.A., Singh, B., Kamal, M., Ahmed, T., Kibria, M. & Chowdhury, N.R. (2022) The role of local topography and sea surface temperature on summer monsoon precipitation over Bangladesh and northeast India. *International Journal of Climatology*, 42(9), 4564–4579. Available from: https://doi.org/10.1002/joc.7490

Feng, P., Liu, D.L., Wang, B., Waters, C., Zhang, M. & Yu, Q. (2019) Projected changes in drought across the wheat belt of southeastern Australia using a downscaled climate ensemble. *International Journal of Climatology*, 39(2), 1041–1053. Available from: https://doi.org/10.1002/joc.5861

Fujinami, H., Hatsuzuka, D., Yasunari, T., Hayashi, T., Terao, T., Murata, F. et al. (2011) Characteristic intraseasonal oscillation of rainfall and its effect on interannual variability over Bangladesh during boreal summer. *International Journal of Climatology*, 31(8), 1192–1204. Available from: https://doi.org/10.1002/joc.2146

Fujinami, H., Sato, T., Kanamori, H. & Kato, M. (2022) Nocturnal southerly moist surge parallel to the coastline over the western Bay of Bengal. *Geophysical Research Letters*, 49(18), e2022GL100174. Available from: https://doi.org/10.1029/2022GL100174

Fujinami, H., Sato, T., Kanamori, H. & Murata, F. (2017) Contrasting features of monsoon precipitation around the Meghalaya Plateau under westerly and easterly regimes. *Journal of Geophysical Research: Atmospheres*, 122(18), 9591–9610. Available from: https://doi.org/10.1002/2016JD026116

Fujinami, H., Yasunari, T. & Morimoto, A. (2014) Dynamics of distinct intraseasonal oscillation in summer monsoon rainfall over the Meghalaya–Bangladesh–western Myanmar region: Covariability between the tropics and mid-latitudes. *Climate Dynamics*, 43, 2147–2166. Available from: https://doi.org/10.1007/s00382-013-2040-1

Gadgil, S. (2003) The Indian monsoon and its variability. *Annual Review of Earth and Planetary Sciences*, 31(1), 429–467. Available from: https://doi.org/10.1146/annurev.earth.31.100901.141251

Ganguly, A., Oza, H., Padhya, V., Pandey, A., Chakra, S. & Deshpande, R.D. (2023) Extreme local recycling of moisture via wetlands and forests in north-east Indian subcontinent: a mini-Amazon. *Scientific Reports*, 13(1), 521. Available from: https://doi.org/10.1038/s41598-023-27577-5

Gibbs, W.J. & Maher, J.V. (1967) Rainfall deciles as drought indicators. In: *Bureau of Meteorology bulletin*, Vol. 48. Melbourne, Vic: Bureau of Meteorology.

Goswami, B.B., Mukhopadhyay, P., Mahanta, R. & Goswami, B.N. (2010) Multiscale interaction with topography and extreme rainfall events in the northeast Indian region. *Journal of Geophysical Research: Atmospheres*, 115, D12114. Available from: https://doi.org/10.1029/2009JD012275

Goswami, B.N. & Mohan, R.S.A. (2001) Intraseasonal oscillations and interannual variability of the Indian summer monsoon. *Journal of Climate*, 14(6), 1180–1198. Available from: https://doi.org/10.1175/1520-0442(2001)014<1180:IOAIVO>2.0.CO;2

Guhathakurta, P., Menon, P., Inkane, P.M., Krishnan, U. & Sable, S.T. (2017) Trends and variability of meteorological drought over the districts of India using standardized precipitation index. *Journal of Earth System Science*, 126(8), 1–18. Available from: https://doi.org/10.1007/s12040-017-0896-x

Guttman, N.B. (1998) Comparing the palmer drought index and the standardized precipitation index. *JAWRA Journal of the American Water Resources Association*, 34(1), 113–121.

Guttman, N.B. (1999) Accepting the standardized precipitation index: a calculation algorithm. *Journal of the American Water Resources Association*, 35(2), 311–322. Available from: https://doi.org/10.1111/j.1752-1688.1999.tb03592.x

Haile, G.G., Tang, Q., Li, W., Liu, X. & Zhang, X. (2020) Drought: Progress in broadening its understanding. *WIREs Water*, 7, 1–25. Available from: https://doi.org/10.1002/wat2.1407

Hari, V., Villarini, G., Karmakar, S., Wilcox, L.J. & Collins, M. (2020) Northward propagation of the intertropical convergence zone and strengthening of Indian summer monsoon rainfall. *Geophysical Research Letters*, 47(23), e2020GL089823. Available from: https://doi.org/10.1029/2020GL089823

Hayes, M.J., Svoboda, M.D., Wilhite, D.A. & Vanyarkho, O.V. (1999) Monitoring the 1996 drought using the standardized precipitation index. *Bulletin of the American Meteorological Society*, 80(3), 429–438. Available from: https://doi.org/10.1175/1520-0477(1999)080<0429:MTDUTS>2.0.CO;2

Hofer, T. & Messerli, B. (2006) *Floods in Bangladesh: history, dynamics and rethinking the role of the Himalayas*. Tokyo: United Nations University Press.

Houze, R.A., Jr. (2012) Orographic effects on precipitating clouds. *Reviews of Geophysics*, 50(1), RG1001. Available from: https://doi.org/10.1029/2011RG000365

Jolliffe, I.T. & Cadima, J. (2016) Principal component analysis: a review and recent developments. *Philosophical Transactions of the Royal Society A: Mathematical, Physical and Engineering Sciences*, 374(2065), 20150202. Available from: https://doi.org/10.1098/rsta.2015.0202

Kad, P. & Ha, K.J. (2023) Recent tangible natural variability of monsoonal orographic rainfall in the eastern Himalayas. *Journal of Geophysical Research: Atmospheres*, 128, e2023JD038759. Available from: https://doi.org/10.1029/2023JD038759

Kamruzzaman, M., Almazroui, M., Salam, M.A., Mondol, M.A.H., Rahman, M.M., Deb, L. et al. (2022) Spatiotemporal drought analysis in Bangladesh using the standardized precipitation index (SPI) and standardized precipitation evapotranspiration index (SPEI). *Scientific Reports*, 12(1), 20694. Available from: https://doi.org/10.1038/s41598-022-24146-0

Kamruzzaman, M., Hwang, S., Cho, J., Jang, M.W. & Jeong, H. (2019) Evaluating the spatiotemporal characteristics of agricultural drought in Bangladesh using effective drought index. *Water*, 11(12), 2437. Available from: https://doi.org/10.3390/w11122437

Kendall, M.G. (1975) *Rank correlation methods*. London: Griffin.

Kirshbaum, D.J. & Smith, R.B. (2008) Temperature and moist-stability effects on midlatitude orographic precipitation. *Quarterly Journal of the Royal Meteorological Society*, 134(634), 1183–1199. Available from: https://doi.org/10.1002/qj.274

Krishnamurthy, V. & Shukla, J. (2000) Intra-seasonal and interannual variability of rainfall over India. *Journal of Climate*, 13, 4366–4377. Available from: https://doi.org/10.1175/1520-0442(2000)013<0001:IAIVOR>2.0.CO;2

Krishnan, R., Sanjay, J., Gnanaseelan, C., Mujumdar, M., Kulkarni, A. & Chakraborty, S. (Eds.). (2020) *Assessment of*

climate change over the Indian region: a report of the ministry of earth sciences (MOES), government of India. Singapore: Springer.

Kumar, A., Sengar, R.S., Pathak, R.K. & Singh, A.K. (2023) Integrated approaches to develop drought-tolerant rice: demand of era for global food security. *Journal of Plant Growth Regulation*, 42, 96–120. Available from: https://doi.org/10.1007/s00344-021-10561-6

Kumar, K.N., Rajeevan, M., Pai, D.S., Srivastava, A.K. & Preethi, B. (2013) On the observed variability of monsoon droughts over India. *Weather and Climate Extremes*, 1, 42–50. Available from: https://doi.org/10.1016/j.wace.2013.07.006

Kumar, M.N., Murthy, C.S., Sesha, S. & Roy, P.S. (2012) Spatiotemporal analysis of meteorological drought variability in the Indian region using standardized precipitation index. *Meteorological Applications*, 19(2), 256–264. Available from: https://doi.org/10.1002/met.277

Kumar, P.V. & Naidu, V.C. (2020) Is pre-monsoon rainfall activity over India increasing in the recent era of global warming? *Pure and Applied Geophysics*, 177, 4423–4442. Available from: https://doi.org/10.1007/s00024-020-02471-7

Kumari, M., Singh, C.K., Bakimchandra, O. & Basistha, A. (2017) Geographically weighted regression based quantification of rainfall–topography relationship and rainfall gradient in Central Himalayas. *International Journal of Climatology*, 37(3), 1299–1309. Available from: https://doi.org/10.1002/joc.4777

Kuttippurath, J., Murasingh, S., Stott, P.A., Sarojini, B.B., Jha, M.K., Kumar, P. et al. (2021) Observed rainfall changes in the past century (1901–2019) over the wettest place on Earth. *Environmental Research Letters*, 16(2), 024018. Available from: https://doi.org/10.1088/1748-9326/abcf78

Liu, C., Yang, C., Yang, Q. & Wang, J. (2021) Spatiotemporal drought analysis by the standardized precipitation index (SPI) and standardized precipitation evapotranspiration index (SPEI) in Sichuan Province, China. *Scientific Reports*, 11(1), 1280. Available from: https://doi.org/10.1038/s41598-020-80527-3

López-Moreno, J.I., Hess, T.M. & White, S. (2009) Estimation of reference evapotranspiration in a mountainous mediterranean site using the Penman–Monteith equation with limited meteorological data. *Pirineos*, 164, 7–31. Available from: https://doi.org/10.3989/pirineos.2009.v164.27

Luo, W., Chen, M., Kang, Y., Li, W., Li, D., Cui, Y. et al. (2022) Analysis of crop water requirements and irrigation demands for rice: implications for increasing effective rainfall. *Agricultural Water Management*, 260, 107285. Available from: https://doi.org/10.1016/j.agwat.2021.107285

Mahanta, R., Sarma, D. & Choudhury, A. (2013) Heavy rainfall occurrences in northeast India. *International Journal of Climatology*, 33(6), 1456–1469. Available from: https://doi.org/10.1002/joc.3526

Mahto, S.S. & Mishra, V. (2020) Dominance of summer monsoon flash droughts in India. *Environmental Research Letters*, 15(10), 104061. Available from: https://doi.org/10.1088/1748-9326/abaf1d

Mahto, S.S. & Mishra, V. (2023) Flash drought intensification due to enhanced land-atmospheric coupling in India. *Journal of Climate*, 22, 1–31. Available from: https://doi.org/10.1175/JCLI-D-22-0477.1

Mallya, G., Mishra, V., Niyogi, D., Tripathi, S. & Govindaraju, R.S. (2016) Trends and variability of droughts over the Indian monsoon region. *Weather and Climate Extremes*, 12, 43–68. Available from: https://doi.org/10.1016/j.wace.2016.01.002

Mann, H.B. (1945) Nonparametric tests against trend. *Econometrica*, 13(3), 245–259. Available from: https://doi.org/10.2307/1907187

Marcos-Garcia, P., Lopez-Nicolas, A. & Pulido-Velazquez, M. (2017) Combined use of relative drought indices to analyze climate change impact on meteorological and hydrological droughts in a Mediterranean basin. *Journal of Hydrology*, 554, 292–305. Available from: https://doi.org/10.1016/j.jhydrol.2017.09.028

McKee, T.B., Doesken, N.J. & Kleist, J. (1993) The relationship of drought frequency and duration to time scales. In: *Proceedings of the 8th conference on applied climatology, 17–22 January 1993*. Wuhan: Scientific Research Publishing, pp. 179–183.

Miah, M.G., Abdullah, H.M. & Jeong, C. (2017) Exploring standardized precipitation evapotranspiration index for drought assessment in Bangladesh. *Environmental Monitoring and Assessment*, 189(11), 1–16. Available from: https://doi.org/10.1007/s10661-017-6235-5

Mishra, A.K. & Singh, V.P. (2010) A review of drought concepts. *Journal of Hydrology*, 391(1–2), 202–216. Available from: https://doi.org/10.1016/j.jhydrol.2010.07.012

Mishra, V. (2020a) Long-term (1870–2018) drought reconstruction in context of surface water security in India. *Journal of Hydrology*, 580, 124228. Available from: https://doi.org/10.1016/j.jhydrol.2019.124228

Mishra, V. (2020b) Relative contribution of precipitation and air temperature on dry season drying in India, 1951–2018. *Journal of Geophysical Research: Atmospheres*, 125, e2020JD032998. Available from: https://doi.org/10.1029/2020JD032998

Misra, V., Bhardwaj, A. & Mishra, A. (2018) Local onset and demise of the Indian summer monsoon. *Climate Dynamics*, 51, 1609–1622. Available from: https://doi.org/10.1007/s00382-017-3924-2

Mondol, M., Haque, A., Ara, I. & Das, S.C. (2017) Meteorological drought index mapping in Bangladesh using standardized precipitation index during 1981–2010. *Advances in Meteorology*, 2017, 4642060. Available from: https://doi.org/10.1155/2017/4642060

Mukherjee, S. & Mishra, A.K. (2021) Increase in compound drought and heatwaves in a warming world. *Geophysical Research Letters*, 48(1), e2020GL090617. Available from: https://doi.org/10.1029/2020GL090617

Murata, F., Hayashi, T., Matsumoto, J. & Asada, H. (2007) Rainfall on the Meghalaya plateau in northeastern India—one of the rainiest places in the world. *Natural Hazards*, 42, 391–399. Available from: https://doi.org/10.1007/s11069-006-9084-z

Murata, F., Terao, T., Fujinami, H., Hayashi, T., Asada, H., Matsumoto, J. et al. (2017) Dominant synoptic disturbance in the extreme rainfall at Cherrapunji, Northeast India, based on 104 years of rainfall data (1902–2005). *Journal of Climate*, 30(20), 8237–8251. Available from: https://doi.org/10.1175/JCLI-D-16-0435.1

Murata, F., Terao, T., Hayashi, T., Asada, H. & Matsumoto, J. (2008) Relationship between atmospheric conditions at Dhaka, Bangladesh, and rainfall at Cherrapunjee, India. *Natural Hazards*, 44, 399–410. Available from: https://doi.org/10.1007/s11069-007-9125-2

Pai, D.S., Arti, B., Sunitha, D., Madhuri, M., Badwaik, M.R., Kundale, A.P. et al. (2020) Normal dates of onset/progress and withdrawal of southwest monsoon over India. *Mausam*, 71(4), 553–570. Available from: https://doi.org/10.54302/mausam.v71i4.33

Pai, D.S., Sridhar, L., Guhathakurta, P. & Hatwar, H.R. (2011) District-wide drought climatology of the southwest monsoon season over India based on standardized precipitation index (SPI). *Natural Hazards*, 59(3), 1797–1813. Available from: https://doi.org/10.1007/s11069-011-9867-8

Palmer, W.C. (1965) *Meteorological drought (Research Paper No. 45)*. Washington, DC: US Weather Bureau.

Pandey, P.K. & Pandey, V. (2016) Evaluation of temperature-based Penman–Monteith (TPM) model under the humid environment. *Modeling Earth Systems and Environment*, 2, 1–10. Available from: https://doi.org/10.1007/s40808-016-0204-9

Paul, A.R. & Maity, R. (2023) Future projection of climate extremes across contiguous northeast India and Bangladesh. *Scientific Reports*, 13(1), 15616. Available from: https://doi.org/10.1038/s41598-023-42360-2

Prokop, P., Kruczkowska, B., Syiemlieh, H.J. & Bucała-Hrabia, A. (2018) Impact of topography and sedentary swidden cultivation on soils in the hilly uplands of North-East India. *Land Degradation & Development*, 29(8), 2760–2770. Available from: https://doi.org/10.1002/ldr.3018

Prokop, P. & Walanus, A. (2003) Trend and periodicity in the longest instrumental rainfall series for the area of most extreme rainfall in the world, northeast India. *Geographia Polonica*, 76(2), 25–35.

Prokop, P. & Walanus, A. (2015) Variation in the orographic extreme rain events over the Meghalaya Hills in northeast India in the two halves of the twentieth century. *Theoretical and Applied Climatology*, 121, 389–399.

Prokop, P. & Walanus, A. (2017) Impact of the Darjeeling–Bhutan Himalayan front on rainfall hazard pattern. *Natural Hazards*, 89, 387–404. Available from: https://doi.org/10.1007/s11069-017-2970-8

Rahman, M.N., Rony, M.R.H. & Jannat, F.A. (2021) Spatiotemporal evaluation of drought trend during 1979–2019 in seven climatic zones of Bangladesh. *Heliyon*, 7(11), e08249. Available from: https://doi.org/10.1016/j.heliyon.2021.e08249

Rajeevan, M., Unnikrishnan, C.K., Bhate, J., Niranjan Kumar, K. & Sreekala, P.P. (2012) Northeast monsoon over India: variability and prediction. *Meteorological Applications*, 19(2), 226–236. Available from: https://doi.org/10.1002/met.1322

Rajesh, P.V., Goswami, B.N., Choudhury, B.A. & Zahan, Y. (2021) Large sensitivity of simulated Indian summer monsoon rainfall (ISMR) to global warming: implications of ISMR projections. *Journal of Geophysical Research: Atmospheres*, 126(1), 1–17. Available from: https://doi.org/10.1029/2020JD033511

Raju, B.M.K., Rao, K.V., Venkateswarlu, B., Rao, A.V.M.S., Rao, C.R., Rao, V.U.M. et al. (2013) Revisiting climatic classification in India: a district-level analysis. *Current Science*, 105(4), 492–495.

Roe, G.H. (2005) Orographic precipitation. *Annual Review of Earth and Planetary Sciences*, 33, 645–671. Available from: https://doi.org/10.1146/annurev.earth.33.092203.122541

Roman-Stork, H.L., Subrahmanyam, B. & Trott, C.B. (2020) Monitoring intraseasonal oscillations in the Indian Ocean using satellite observations. *Journal of Geophysical Research: Oceans*, 125(2), e2019JC015891. Available from: https://doi.org/10.1029/2019JC015891

Romatschke, U. & Houze, R.A. (2011) Characteristics of precipitating convective systems in the South Asian monsoon. *Journal of Hydrometeorology*, 12(1), 3–26. Available from: https://doi.org/10.1175/2010JHM1289.1

Romatschke, U., Medina, S. & Houze, R.A., Jr. (2010) Regional, seasonal, and diurnal variations of extreme convection in the South Asian region. *Journal of Climate*, 23(2), 419–439. Available from: https://doi.org/10.1175/2009JCLI3140.1

Rotunno, R. & Houze, R.A. (2007) Lessons on orographic precipitation from the Mesoscale Alpine Programme. *Quarterly Journal of the Royal Meteorological Society*, 133(625), 811–830. Available from: https://doi.org/10.1002/qj.67

Rouault, M. & Richard, Y. (2003) Intensity and spatial extension of drought in South Africa at different time scales. *Water SA*, 29(4), 489–500. Available from: https://doi.org/10.4314/wsa.v29i4.5057

Sahany, S., Mishra, S.K., Pathak, R. & Rajagopalan, B. (2018) Spatiotemporal variability of seasonality of rainfall over India. *Geophysical Research Letters*, 45(14), 7140–7147. Available from: https://doi.org/10.1029/2018GL077932

Samuel, S., Mathew, N. & Sathiyamoorthy, V. (2023) Characterization of intertropical convergence zone using SAPHIR/Megha-Tropiques satellite brightness temperature data. *Climate Dynamics*, 60(11–12), 3765–3783. Available from: https://doi.org/10.1007/s00382-022-06549-x

Sato, T. (2013) Mechanism of orographic precipitation around the Meghalaya Plateau associated with intraseasonal oscillation and the diurnal cycle. *Monthly Weather Review*, 141(7), 2451–2466. Available from: https://doi.org/10.1175/MWR-D-12-00321.1

Sen, P.K. (1968) Estimates of the regression coefficient based on Kendall's tau. *Journal of the American Statistical Association*, 63(324), 1379–1389. Available from: https://doi.org/10.1080/01621459.1968.10480934

Shahfahad Talukdar, S., Ghose, B., Islam, A.R.M.T., Hasanuzzaman, M., Ahmed, I.A., Praveen, B. et al. (2023) Predicting long term regional drought pattern in Northeast India using advanced statistical technique and wavelet-machine learning approach. *Modeling Earth Systems and Environment*, 10, 1005–1026. Available from: https://doi.org/10.1007/s40808-023-01818-y

Shahid, S. (2010) Rainfall variability and the trends of wet and dry periods in Bangladesh. *International Journal of Climatology*, 30(15), 2299–2313. Available from: https://doi.org/10.1002/joc.2053

Singh, S., Hayashi, T., Syiemlieh, H.J., Cajee, L. & Terao, T. (2011) Weather variability and rainfall pattern of Sidr, the post-monsoon cyclonic storm of 15 November 2007 in the Meghalaya Plateau, India. *Current Science*, 100, 1522–1531.

Sneyers, R. (1990) *On statistical analysis of series of observations*. Geneva: World Meteorological Organization. WMO technical note 143.

Stevens, B. (2005) Atmospheric moist convection. *Annual Review of Earth and Planetary Sciences*, 33, 605–643. Available from: https://doi.org/10.1146/annurev.earth.33.092203.122658

Svoboda, M.D. & Fuchs, B.A. (2016) *Handbook of drought indicators and indices*, Vol. 2. Geneva: World Meteorological Organization.

Syroka, J. & Toumi, R. (2004) On the withdrawal of the Indian summer monsoon. *Quarterly Journal of the Royal Meteorological Society*, 130(598), 989–1008. Available from: https://doi.org/10.1256/qj.03.36

Tadić, L., Bonacci, O. & Brleković, T. (2019) An example of principal component analysis application on climate change assessment. *Theoretical and Applied Climatology*, 138, 1049–1062. Available from: https://doi.org/10.1007/s00704-019-02887-9

Tawde, S.A. & Singh, C. (2015) Investigation of orographic features influencing spatial distribution of rainfall over the Western Ghats of India using satellite data. *International Journal of Climatology*, 35(9), 2280–2293. Available from: https://doi.org/10.1002/joc.4146

Trnka, M., Dubrovský, M., Svoboda, M., Semerádová, D., Hayes, M., Žalud, Z. et al. (2009) Developing a regional drought climatology for The Czech Republic. *International Journal of Climatology*, 29(6), 863–883. Available from: https://doi.org/10.1002/joc.1745

Uddin, M.J., Hu, J., Islam, A.R.M.T., Eibek, K.U. & Nasrin, Z.M. (2020) A comprehensive statistical assessment of drought indices to monitor drought status in Bangladesh. *Arabian Journal of Geosciences*, 13, 1–10. Available from: https://doi.org/10.1007/s12517-020-05302-0

Vaid, S.K. (2020) An overview of Indian agriculture with focus on challenges and opportunities in North East. In: Goel, R., Soni, R., & Suyal, D. (Eds.) *Microbiological advancements for higher altitude agro-ecosystems & sustainability. Rhizosphere biology*. Singapore: Springer, pp. 15–36.

Varikoden, H. & Revadekar, J.V. (2020) On the extreme rainfall events during the southwest monsoon season in northeast regions of the Indian subcontinent. *Meteorological Applications*, 27(1), e1822. Available from: https://doi.org/10.1002/met.1822

Ventura, S., Miró, J.R., Peña, J.C. & Villalba, G. (2023) Analysis of synoptic weather patterns of heatwave events. *Climate Dynamics*, 61, 4679–4702. Available from: https://doi.org/10.1007/s00382-023-06828-1

Vicente-Serrano, S.M., Beguería, S. & López-Moreno, J.I. (2010) A multiscalar drought index sensitive to global warming: the standardized precipitation evapotranspiration index. *Journal of Climate*, 23(7), 1696–1718. Available from: https://doi.org/10.1175/2009JCLI2909.1

Vicente-Serrano, S.M. & Beguería-Portugués, S. (2003) Estimating extreme dry-spell risk in the middle Ebro valley (northeastern Spain): a comparative analysis of partial duration series with a general Pareto distribution and annual maxima series with a Gumbel distribution. *International Journal of Climatology*, 23(9), 1103–1118. Available from: https://doi.org/10.1002/joc.934

Vishnu, S., Chakraborty, A. & Srinivasan, J. (2022) Why the droughts of the Indian summer monsoon are more severe than the floods. *Climate Dynamics*, 58(11–12), 3497–3512. Available from: https://doi.org/10.1007/s00382-021-06111-1

Wable, P.S., Jha, M.K. & Shekhar, A. (2019) Comparison of drought indices in a semi-arid river basin of India. *Water Resources Management*, 33, 75–102. Available from: https://doi.org/10.1007/s11269-018-2089-z

Wilhite, D.A. & Glantz, M.H. (1985) Understanding: the drought phenomenon: the role of definitions. *Water International*, 10(3), 111–120. Available from: https://doi.org/10.1080/02508068508686328

World Bank Bangladesh. (1998) *Water resource management in Bangladesh: steps towards a new national water plan*. Dhaka: World Bank. Report No. 17663-BD.

Xie, H., Ringler, C., Zhu, T. & Waqas, A. (2013) Droughts in Pakistan: a spatiotemporal variability analysis using the Standardized Precipitation Index. *Water International*, 38(5), 620–631. Available from: https://doi.org/10.1080/02508060.2013.827889

Xie, S.P., Xu, H., Saji, N.H. & Wang, Y. (2006) Role of narrow mountains in large-scale organization of Asian monsoon convection. *Journal of Climate*, 19, 3420–3429. Available from: https://doi.org/10.1175/JCLI3777.1

Yevjevich, V. (1967) *An objective approach to definitions and investigations of continental hydrologic droughts*. Fort Collins, CO: Colorado State University. Hydrology papers 23.

Yue, S. & Wang, C. (2004) The Mann–Kendall test modified by effective sample size to detect trend in serially correlated hydrological series. *Water Resources Management*, 18(3), 201–218. Available from: https://doi.org/10.1023/B:WARM.0000043140.61082.60

How to cite this article: Prokop, P., & Walanus, A. (2024). Orographic effects on droughts in a monsoon climate with the world's highest rainfall. *International Journal of Climatology*, *44*(7), 2438–2461. https://doi.org/10.1002/joc.8462